Available online at www.sciencedirect.com
ScienceDirect
Global and Planetary Change 61 (2008) 151–174
GLOBAL AND PLANETARY CHANGE
www.elsevier.com/locate/gloplacha

# Influence of substrate tectonic heritage on the evolution of composite volcanoes: Predicting sites of flank eruption, lateral collapse, and erosion

Alessandro Tibaldi [a,*], Claudia Corazzato [a], Andrey Kozhurin [b], Alfredo F.M. Lagmay [c], Federico A. Pasquarè [d], Vera V. Ponomareva [b], Derek Rust [e], Daniel Tormey [f], Luigina Vezzoli [d]

[a] *Università degli Studi di Milano-Bicocca, Dipartimento di Scienze Geologiche e Geotecnologie, Milan, Italy*
[b] *Institute of Volcanology and Seismology, Petropavlovsk-Kamchatsky, Russia*
[c] *National Institute of Geological Sciences, Quezon City, Philippines*
[d] *Università degli Studi dell'Insubria, Dipartimento di Scienze Chimiche e Ambientali, Como, Italy*
[e] *School of Earth and Environmental Sciences, University of Portsmouth, UK*
[f] *ENTRIX Inc., Ventura, California, USA*

Received 30 January 2007; accepted 23 August 2007
Available online 9 October 2007

**Abstract**

This paper aims to aid understanding of the complicated interplay between construction and destruction of volcanoes, with an emphasis on the role of substrate tectonic heritage in controlling magma conduit geometry, lateral collapse, landslides, and preferential erosion pathways. The influence of basement structure on the development of six composite volcanoes located in different geodynamic/geological environments is described: Stromboli (Italy), in an island arc extensional tectonic setting, Ollagüe (Bolivia–Chile) in a cordilleran extensional setting, Kizimen (Russia) in a transtensional setting, Pinatubo (Philippines) in a transcurrent setting, Planchon (Chile) in a compressional cordilleran setting, and Mt. Etna (Italy) in a complex tectonic boundary setting. Analogue and numerical modelling results are used to enhance understanding of processes exemplified by these volcanic centres. We provide a comprehensive overview of this topic by considering a great deal of relevant, recently published studies and combine these with the presentation of new results, in order to contribute to the discussion on substrate tectonics and its control on volcano evolution. The results show that magma conduits in volcanic rift zones can be geometrically controlled by the regional tectonic stress field. Rift zones produce a lateral magma push that controls the direction of lateral collapse and can also trigger collapse. Once lateral collapse occurs, the resulting debuttressing produces a reorganization of the shallow-level magma migration pathways towards the collapse depression. Subsequent landslides and erosion tend to localize along rift zones. If a zone of weakness underlies a volcano, long-term creep can occur, deforming a large sector of the cone. This deformation can trigger landslides that propagate along the destabilized flank axis. In the absence of a rift zone, normal and transcurrent faults propagating from the substrate through the volcano can induce flank instability in directions respectively perpendicular and oblique to fault strike. This destabilization can evolve to lateral collapse with triggering mechanisms such as seismic activity or magmatic intrusion.


*Keywords:* volcano; basement; eruption; lateral collapse; erosion

## 1. Introduction

Volcanoes have the highest accumulation rates of surficial geological features. Edifices as high as 2 km can be emplaced within time spans on the order of 10 ka (Braitseva et al., 1995). Volcanic landscapes can change at dramatically higher rates than other geological environments, due both to constructional processes and destructional ones such as lateral collapses and landslides. Volcanic debris avalanches resulting from lateral collapse are the largest landslide events on Earth (McGuire, 1996), yielding deposits ranging from 1 $km^3$ to 30 $km^3$. Recent findings show that at single large volcanoes, the occurrence of multiple debris avalanches seems to be a common feature with 2 to 14 events during their lifetime (10–500 ka) (Beget and Kienle, 1992; Tibaldi et al., 2005). In areas of high magma

* Corresponding author.
*E-mail address:* alessandro.tibaldi@unimib.it (A. Tibaldi).

0921-8181/$ - see front matter © 2007 Elsevier B.V. All rights reserved.
doi:10.1016/j.gloplacha.2007.08.014

production, recurrence intervals of lateral collapse in a volcanic complex can be on the order of 30 to a few hundred years (Tibaldi et al., 2005). The occurrence of lateral collapses also strongly influences the local geomorphology; for example, damming of rivers with subsequent formation of lacustrine environments, followed by periods of high sediment transport along river segments, as observed after the 1980 eruption of Mount St. Helens (Voight et al., 1981). Volcanic debris avalanches can also cause the destruction of natural environments and urban areas, while destructive tsunamis caused by volcanic debris avalanches from coastal and island volcanoes are responsible for the majority of fatalities from this phenomenon (Siebert, 1996). Increasingly intense rainfall and melting of summit glaciers due to global climate change may produce a greater incidence of such events, through increased fluid circulation, loss of substrate cohesion, increased edifice mass and destabilization of oversteepened slopes.

Lateral collapse is shown to occur in a direction perpendicular to the trend of preferential dyking within a volcano, as demonstrated by field studies, and numerical and analogue modelling (Lipman et al., 1981; Moore and Albee, 1981; Siebert et al., 1987; Tibaldi, 1996, 2001; Voight and Elsworth, 1997; Voight, 2000; Donnadieu et al., 2001; Tibaldi et al., 2006). The orientation of a dyking zone, commonly defined as a volcanic rift zone, is usually attributed to basement structure (Nakamura et al., 1977; Walker, 1999). Other authors attribute rift zones in large volcanoes to shallow-level volcano stress distribution rather than basement structure (Fiske and Jackson, 1972). In the special case of a mechanically weak area of the volcano basement, gravity sliding or volcanic spreading have been proposed to control the formation of rift zones and the subsequent structural evolution of the volcano (Borgia et al., 2000a,b).

Depressurization caused by lateral collapse can in turn alter the shallow magma feeder system, controlling the location and configuration of new craters and dyke paths (Tibaldi, 1996, 2004; Walter and Troll, 2003; Acocella and Tibaldi, 2005). Therefore, magma injection and lateral collapse appear to be intimately connected, both in terms of orientation and triggering mechanism.

This paper aims to decipher the complicated interplay between volcanic construction and destruction, with emphasis on the role of substrate tectonic heritage in controlling the geometry of magma pathways, lateral collapse, and preferential erosion pathways. Recent published field and modelling studies are combined with our new results, to provide a comprehensive discussion. We would like to point out that wherever in the present text data and observations are presented but no bibliographic reference is provided, it is implied that these data were collected by the present authors and are here published for the first time. Large volcanic landslides pose a significant risk to human settlements and other ecosystems, and their incidence can be altered as a result of climate change. The findings summarized in this paper will therefore support assessment of volcanic hazards to human society and environmental resources. Six volcanoes studied in the framework of an International Lithosphere Program project, encompassing different geodynamic, geological and natural environments, provide data leading to our findings: Stromboli (Italy), located in an island arc extensional tectonic setting, Ollagüe (Bolivia–Chile) in a cordilleran extensional setting, Kizimen (Russia) in a transtensional setting, Pinatubo (Philippines) in a transcurrent setting, Planchon (Chile) in a compressional cordilleran setting, and Mt. Etna (Italy) in a complex tectonic boundary setting. Analogue and numerical modelling results simulating these processes are used to enhance the field studies.

## 2. Field data on key volcanoes

### 2.1. Stromboli (Italy)

Stromboli is the northernmost volcano of the Aeolian Arc (Fig. 1A) in the southern Tyrrhenian Sea. Stromboli Island represents the emerged part of an active composite volcano, with an elevation of about 2.6 km above the sea floor (Gabbianelli et al., 1993), and located on a 20-km thick continental crustal sector where NW–SE-directed extension occurs (Tibaldi, 2004; Billi et al., 2006). The rock composition spans basaltic andesite to shoshonite and to latite-trachyte (Hornig-Kjiarsgaard et al., 1993), with the oldest exposed products dating back to about 100 ka (Gillot and Keller, 1993) (Fig. 1B). Volcano growth was repeatedly interrupted by three caldera collapses and five lateral collapse events, followed by reorganizations of eruptive centres (Pasquarè et al., 1993; Tibaldi et al., 1994) (Fig. 1C). Between 85 and 64 ka an initial summit caldera collapse was caused by explosive eruptions. After a phase of cone growth, the SE flank of the edifice was affected by a relatively small lateral collapse dated between 35 and 26 ka. In the same time interval, a second summit caldera collapse was caused by an explosive eruption that produced extensive pyroclastic deposits; this was followed by another phase of cone growth. The third summit caldera collapse took place between 26 and 21 ka and a new cone grew from this time until 13 ka, marking an important transition in volcanic and collapse characteristics. From this time onwards, lateral collapses only developed on the NW side of the volcano, alternating with phases of cone growth. The collapses formed nested horseshoe-shaped amphitheatres open to the northwest; the present-day Sciara del Fuoco depression is the most recent one.

The deformation style accompanying the various growth phases was primarily fracturing and intrusive dyke sheeting along a NE-trending rift zone crossing the Stromboli volcano summit (Fig. 1C). This orientation coincides with the strike of regional faulting close to or beneath the edifice (Gabbianelli et al., 1993; Billi et al., 2006). Within this rift zone, single sheets strike between NNE and ENE. Relationships between the unconformity surfaces of the various growth phases and these sheets indicate that the NE-trending rift zone endured for the volcano's entire history, with a migration of intrusive activity northeast-wards along the rift. Only two growth phases were accompanied by intrusions with a different geometry. The first occurred before the oldest caldera collapse and was characterised by formation of a N–S sheet swarm (64–36 ka). The second different sheet geometry occurred after the oldest (13 ka) lateral collapse towards the NW and was characterised by sheeting parallel to the amphitheatre scarps of this lateral

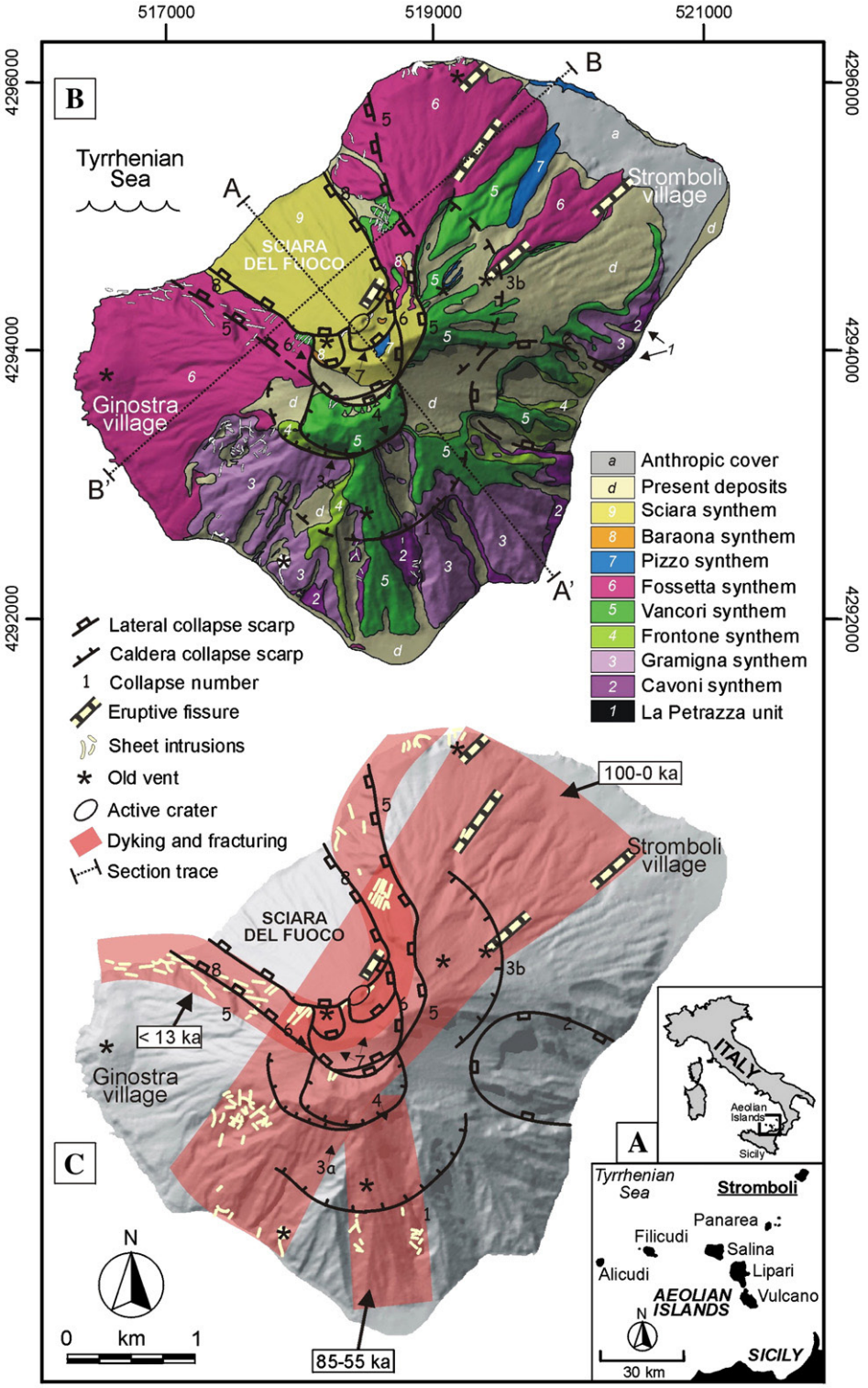


Fig. 1. A. Location of Stromboli in the regional context of the southern Tyrrhenian sea and the Aeolian Archipelago. B. Simplified geologic map of Stromboli based on geological surveys by A. Tibaldi. C. Structural sketch map. The volcano growth was repeatedly interrupted by caldera collapses in the time span 85.3–21 ka. Between 35 and 26 ka, a relatively small flank collapse developed towards SE. After 13 ka, four lateral collapses developed towards NW, alternated by cone growth phases. The deformation system accompanying the various growth/collapse phases was primarily fracturing and intrusive sheeting along a NE-trending rift zone crossing the volcano summit, but after 13 ka dykes mostly intruded along and within the NW lateral collapse zone and in the northeastern part of the NE–SW rift zone.

collapse and along the NE-trending weakness zone. The same geometry characterises the fracture systems.

A shifting of the intrusive/eruptive activity towards the north-western volcano flank is another important change that occurred after the development of the first lateral collapse towards the NW at 13 ka. This shift is expressed by: 1) the presence of eruptive centres and dykes younger than 13 ka along the NE rift zone and in the north-western half of the

volcano, and centres/dykes older than 13 ka in the southeastern half of the volcano, and 2) a northwest shift, by some hundred metres, of the main summit crater zone during Pleistocene to Holocene times (Tibaldi, 2001).

### 2.2. Ollagüe (Bolivia–Chile)

Ollagüe is an active composite volcano located in the Central Andes (21°18'S, 68°11'W, Fig. 2) at the boundary between the Western Cordillera (Quaternary–Present magmatic arc; de Silva and Francis, 1991) and the Altiplano–Puna plateau (crustal thickness ~70 km; Schmitz et al., 1999). The substrate structure is characterized by a series of NW-striking faults belonging to the Pastos Grandes–Lipez–Coranzuli system. These structures consist of left-lateral strike–slip faults, often reactivated with extensional motions (Riller et al., 2001; Acocella et al., 2007). These tectonic features are well expressed in the dominant NW-trending alignment of andesite–dacite composite volcanoes, rhyolite–dacite ignimbrite-forming calderas and voluminous monogenetic lava flows and domes (de Silva, 1989; de Silva et al., 1994), and small basalt monogenetic scoria cones and lava flows (Davidson and de Silva, 1992; Kay et al., 1994; Mattioli et al., 2006).

The long-lived (1.2 Ma — Present) Ollagüe volcano (5868 m a.s.l.) has products ranging from few basaltic andesites to mainly andesites and dacites, defining a high-K calc-alkaline suite (Feeley et al., 1993; Feeley and Davidson, 1994; Wörner et al., 1992; 2000). Investigation undertaken by the present authors (Tibaldi et al., 2006) pointed out stratigraphic and structural relationships, with new petrographic, geochemical and $^{40}Ar$–$^{39}Ar$ geochronological data. The data outline the evolution of Ollagüe, define multiple lateral collapse events, and demonstrate a strict control by the substrate structures on volcanic slope failures and the shallow magmatic system. Ollagüe's' geological history is characterized by four stages of volcano construction separated by three main events of cone deformation and failure (Fig. 2) controlled by the regional NW-striking extensional fault system underlying the edifice. The deformation progresses from: a) downthrow of the SW sector of the volcano (~750 ka) along the NW-striking normal fault propagating from the substrate; b) development of lateral narrow collapses along the fault strike (~450 ka), along which fracturing and deformation focused and lateral and parasitic eruptive vents concentrated; c) final catastrophic failure (~200 ka) of the SW sector. Two of these collapse events can be correlated with debris avalanche emplacement: At the distal (western) base of Ollagüe, two debris avalanche deposits crop out with typical hummocky topography, a minimum area of 80 $km^2$, an extent of 20 km from the volcano summit crater, and an estimated volume of 1 $km^3$ for the younger deposit (Francis and Wells, 1988; Feeley et al., 1993; Clavero et al., 2004).

During the four stages of Ollagüe's growth, central vents shifted SW, that is perpendicular to the NW-striking substrate fault and along the axis of the older lateral collapse. At the end of the second lateral collapse (~450 ka), several lateral vents, including the parasitic dacite lava domes/flows of La Celosa and Chaska Orkho, developed on the lower slopes of the cone along a NW-trending belt, sub-parallel to the NW-striking normal fault and collapse scarps. Finally, the active Ollagüe edifice (200 ka–Present) is characterized by lateral lava flows extruded along the axis of the lateral collapse amphitheatre, and a range of NW-aligned and SE-wards younging sub-terminal lava domes. This NW-alignment of lateral vents suggests the presence of a NW-trending feeder dyke beneath the volcano, intruded along the substrate fault, which may have served as a principal conduit for magma ascent and surface eruptions. In addition, the unbuttressing due to the development of lateral collapses focused the propagation of the dyke and the shifting of magmatic activity within and around Ollagüe's collapse amphitheatre.

### 2.3. Planchon (Chile)

The active volcanic complex of Azufre–Planchon–Peteroa is located in remote, steeply glaciated terrain on the crest of the Chilean Andes along the active volcanic front at 35°15'S. Dissection by glaciers and lateral collapse provide spectacular exposure of this still-active volcanic system, and allows study of stratigraphic sections and collection of samples with known relative age (Tormey et al., 1989, 1995; Naranjo and Haller, 2002). From 35°S to 37°S, the Andean magmatic arc consists of a NNE-trending volcanic front, a N-trending series of large rhyolitic calderas and dome complexes extending approximately 30 km to the east (Hildreth et al., 1999), and a zone of extension-related alkali basalt fields 50 to 100 km to the east of the volcanic front (Bermùdez and Delpino, 1989). The volcanic front was developed in a compressional stress regime as part of the Mallargue fold and thrust belt from Miocene to Pliocene (Ramos et al., 1996; Hildreth et al., 1999). The basement structures are dominated by reverse faults striking approximately N–S. Folguera et al. (2006a) have identified a series of Pliocene to Quaternary back-arc extensional basins that, in the vicinity of Azufre–Planchon–Peteroa, consist of the Las Loicas trough. This feature intersects the volcanic front and appears to be partially filled by eruptive products from the active volcanic complex. As such, much of the development of the volcanic complex is likely to have been in a compressional cordilleran setting (Hildreth et al., 1999; Kay et al., 2005; Folguera et al., 2006a).

The volcanic complex is less than 0.55 Ma old and consists of the long-lived polycyclic basaltic andesite to dacite Volcan Azufre (69 $km^3$), followed by the relatively short-lived basalt to basaltic andesite Volcan Planchon (43 $km^3$) and the more recent Volcan Peteroa (Tormey et al., 1995; Fig. 3). Planchon is 6 km north of Azufre, and its lavas are sheet-like and do not fill obvious topographic features; there are also no intercalations of sediment within the flow succession. It appears, therefore, that flows were not channelized, the growth of the volcano was not interrupted by glaciation, and the construction of Planchon was rapid enough to prevent deep erosion during growth.

Approximately 9 ka ago (MacPhail, 1973), a 30° sector of Planchon and part of Azufre collapsed to form a debris avalanche that travelled 75 km west forming a hummocky deposit approximately 10 $km^3$ in volume known as the Rio Teno Debris Avalanche (MacPhail, 1973; Davidson, 1974; Scott et al., 2001). The lateral collapse depression is open to the west, perpendicular to the major substrate tectonic structures in the region. The debris

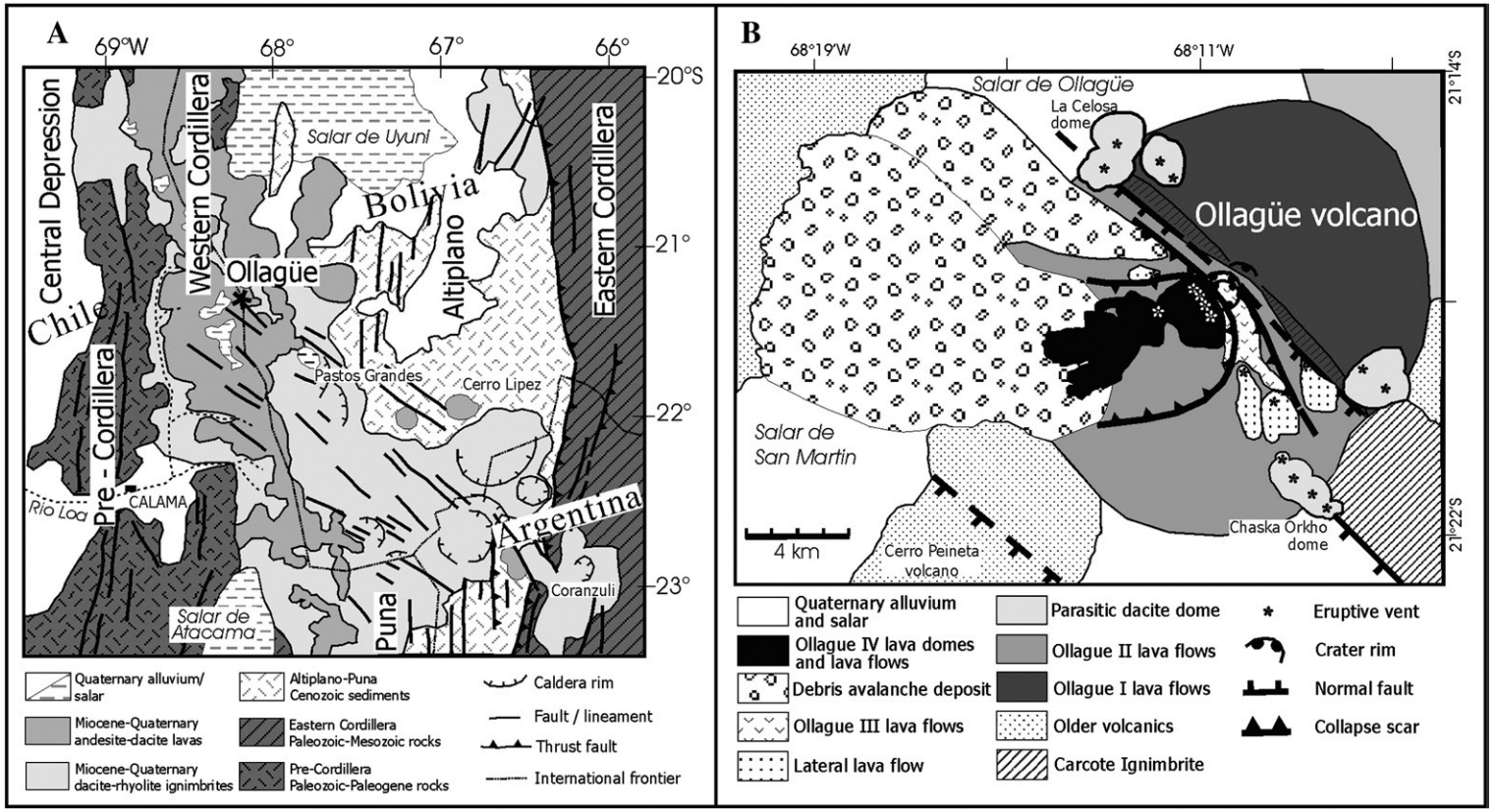


Fig. 2. A. Geologic sketch map of the Central Andes, showing the main N–S-trending structural units intersected by the NW-striking Pastos Grandes–Lipez–Coranzuli fault system. The Ollagüe volcano rose at the intersection between the active magmatic arc of the Western Cordillera and this transversal structural lineament. B. Geological map of the Ollagüe volcano, showing the four phases of volcano activity and the multiple lateral collapses. Alignment of the volcanic structures and vents are either parallel with, or perpendicular to, the NW-striking normal fault that bisects the cone.

avalanche deposit appears to preserve at least two distinct pulses of flow, and shows grain-size gradation both laterally and longitudinally. Based on the area excavated by the lateral collapse, approximately 3 to 4 km$^3$ of material was derived from the volcanic edifice while the remainder appears to have been alluvial deposits entrained during flow by bulking, greatly increasing the volume and mobility of the debris avalanche.

In a geochemical study of this volcanic centre, Tormey et al. (1995) documented that most basalt and basaltic andesite lavas erupted from Planchon evolved at mid-crustal depths of approximately 12 to 18 km. Just prior to the collapse, however, a series of mafic lava flows indicate shallow-level fractional crystallization and assimilation of shallow crustal wall rocks. Although the depth cannot be constrained with certainty because a lower water pressure would give a similar compositional trend, it is likely to be within the upper 3 km of the crust (Tormey et al., 1995). Although the development of a shallow magma body may have led to lateral collapse and debris avalanche by weakening the mechanical properties of the edifice, either through enhanced hydrothermal activity or melting of the summit ice cap, the data do not prove this relationship.

After the collapse, a new edifice, Planchon II, developed within the collapse amphitheatre, 1 km south of Planchon (Fig. 3). The compositional variation of Planchon II basalt and basaltic andesite lavas reverted to those indicative of mid-crustal (12 to 18 km depth) evolution; these lavas are compositionally indistinguishable from the early lavas of Planchon. It is not clear whether the collapse caused the cessation of shallow-level magma storage, but the post-collapse lavas clearly erupted without the imprint of shallow-level crystallization and assimilation.

The Planchon II edifice was rapidly dissected by landslides and erosion, which mostly developed perpendicular to the tectonically controlled N–S axis. Presently, the Planchon II edifice is only preserved as ramparts of radially-dipping lavas. Planchon II has a larger proportion of near-vent pyroclastic deposits than Planchon; this structural weakness may have contributed to the rapid destruction of the cone, in a similar way to Stromboli (Tibaldi, 2001; Apuani et al., 2005a).

The most recent activity of the volcanic complex produced Volcan Peteroa, which encompasses several scattered vents along the north–south axis of Azufre and Planchon that have erupted calc-alkaline andesites, dacites, and rhyodacites.

### 2.4. Kizimen (Russia)

Kizimen is a composite volcano (Shantser et al., 1991) located in the Central Kamchatka depression (Russia) between the eastern volcanic front and the northern volcanic zone (Fig. 4A). It is on the edge of the southeastern flank of the Shchapinskiy graben, a

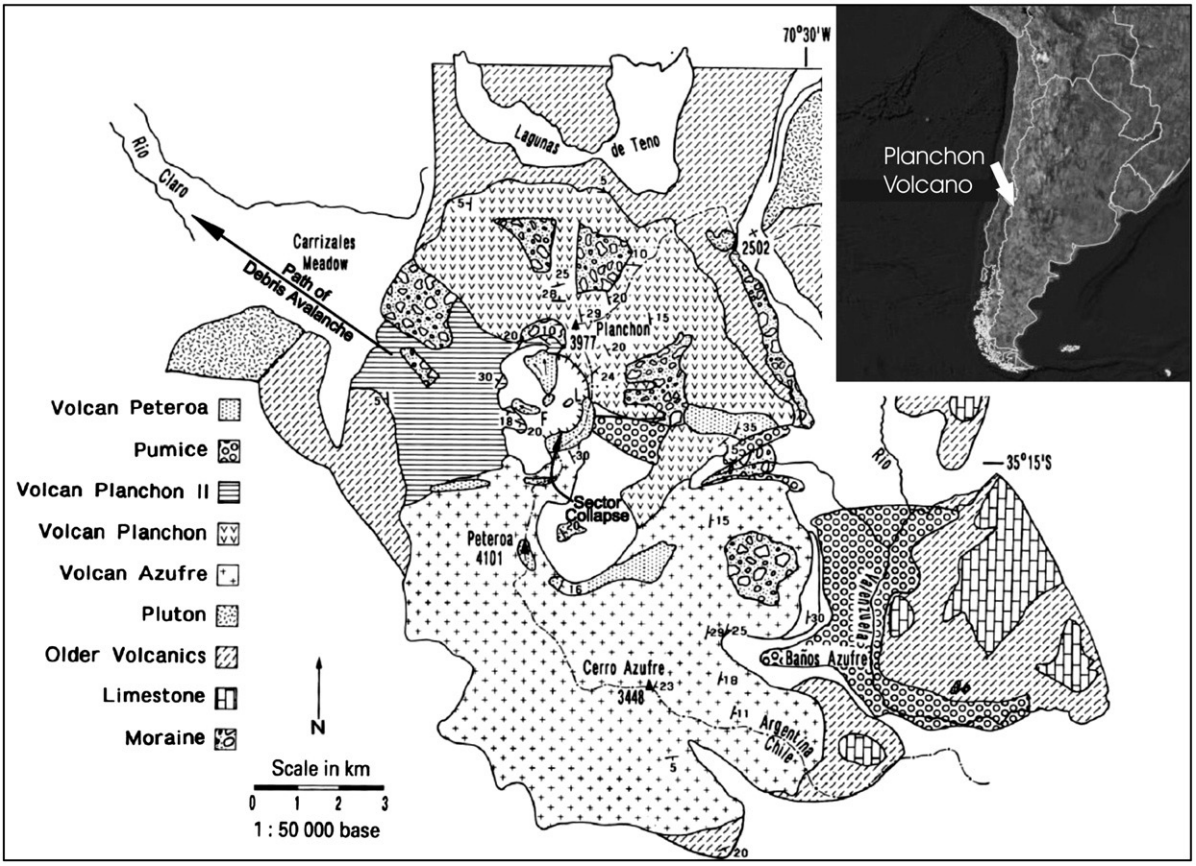


Fig. 3. Geological sketch map of the active volcanic complex of Azufre–Planchon–Peteroa, from Tormey et al., 1995. The volcanic complex is less than 0.55 Ma and consists of polycyclic basaltic andesite to dacite Volcan Azufre (69 km$^3$), followed by the relatively short-lived basalt to basaltic andesite Volcan Planchon (43 km$^3$) and the active Peteroa volcano. Note the shifting of the main volcanic centre of Planchon towards the south to form Planchon II, towards the summit amphitheatre formed by the lateral collapse.

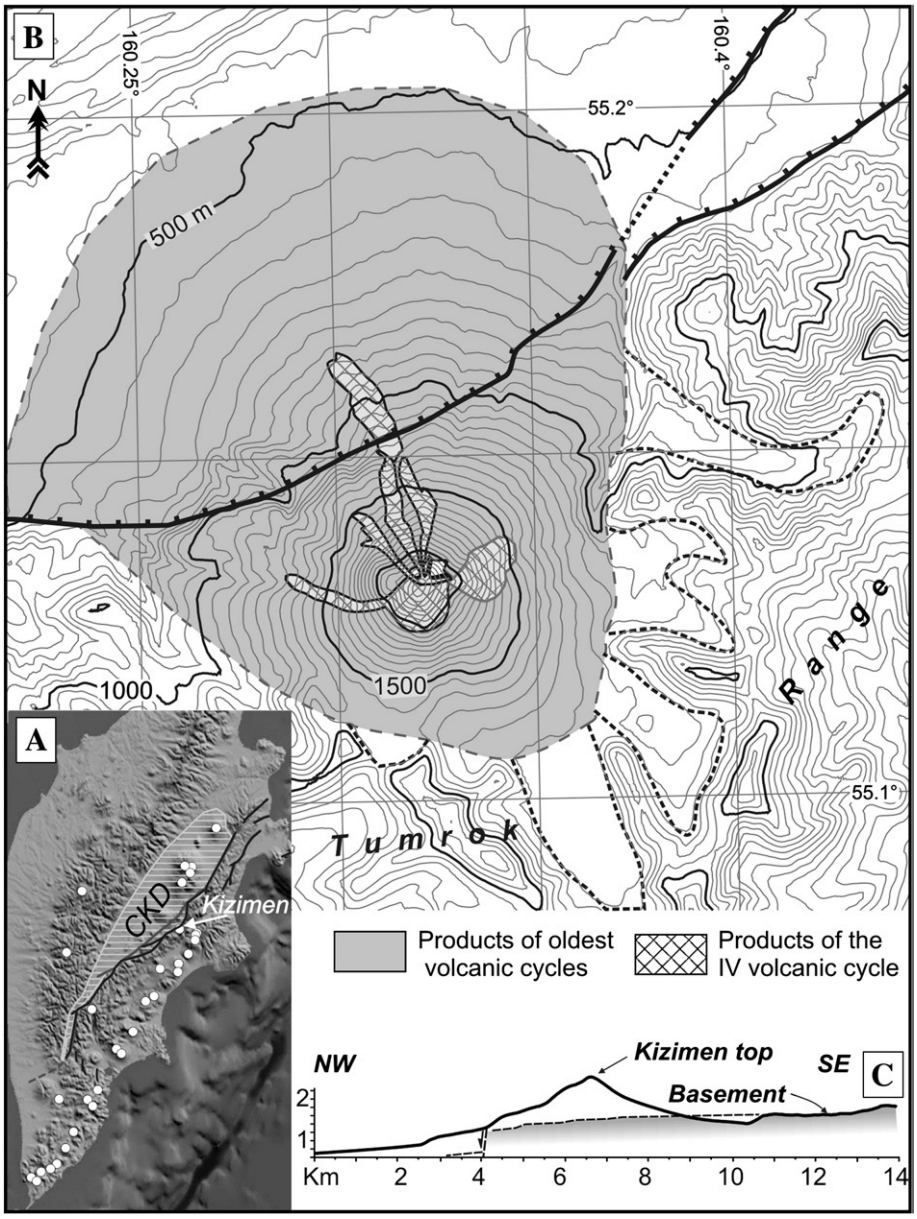


Fig. 4. A. Location of Kizimen composite volcano within the Central Kamchatka Depression, Russia (CKD). Thick black lines are active faults of the East Kamchatka fault zone, white circles are active volcanoes. B. Geological sketch of the volcano and main faults. At the centre, extrusive domes and lava flows of cycle 4 of the volcano growth are shown. Black thick lines with bars are active normal faults (bars on downthrown side). Topographic contour interval is 50 m. Thick dashed lines border the upper parts of large flat bottomed valleys, likely of glacial nature, dammed by the volcanic cone. C. Schematic section showing the possible geometry of the substrate offset by the main fault.

NNE-striking tectonic depression bordered to the east by WNW-dipping master normal faults which belong to the East Kamchatka fault zone and have a minor component of transcurrent motion (Kozhurin, 2004). The footwall fault block, which constitutes the graben shoulder and also the substrate of the volcano, is composed of volcanic and volcano-derived sedimentary rocks of the Upper Miocene Shchapinsky succession and of volcanic rocks of Late Pliocene–Pleistocene age (Shantser et al., 1969).

New field data reveal a sequence of tectonic, erosion and volcanic events that characterised the evolution of the area. The areal distribution of the older rocks and their relationship to the graben faults indicate that the formation and development of the graben started in the Middle Quaternary. Widespread "roches moutonnées", glacial abrasion surfaces and deposits, and related morphologic features along the fault scarps indicate that erosional modification of the uplifted blocks took place primarily during Late Pleistocene glaciations. These were followed by the onset of volcanic activity in the Late Pleistocene that formed Kizimen volcano. Since the entire volcano is crossed by a fault aligned with the main fault bordering the graben depression, it must be concluded that fault activity rejuvenated after or during the volcano emplacement (Fig. 4).

Radiocarbon dating of paleosoils interlayered with explosive deposits erupted from this volcano indicate that four main cycles of volcanic activity occurred, each 2 to 3.5 ka in duration. The onset of the first of these dates back to 11–12 ka ago. Each

of the cycles started with high activity followed by decreasing activity and then a generally quiet period. The duration of these cycles corresponds to recurrence intervals of up to 3.5 ka between faulting events on one of the main faults of the East Kamchatka fault zone located north of this volcano (Kozhurin et al., 2006).

The fault scarp passing through the volcano flank is 50 m (in the northeast) to 200 m (in the southwest) high. These values are lower than those measured along the fault in the substrate surrounding the volcano, indicating that normal faulting here started before volcano construction and then increments of faulting occurred during the various growth stages. Although the fault tips on the volcano correspond to the zone where the graben fault passes beneath the volcano edifice (Fig. 4B,C), it is noteworthy that the fault trace on the volcano is curved in plan view, with the concave side facing towards the NW. This fault cuts lava flows from the initial stage of the fourth (last) cycle, which lasted from about 3 ka to 1.9 ka. Younger lava flows of the second stage of this cycle have been dated to about 1.1 ka; since these flows did not reach the fault, it is difficult to determine if the last tectonic motion along this fault post-dates or pre-dates these very young lava flows.

Although part of the normal faulting appears to have accompanied the volcano construction, no debris avalanche

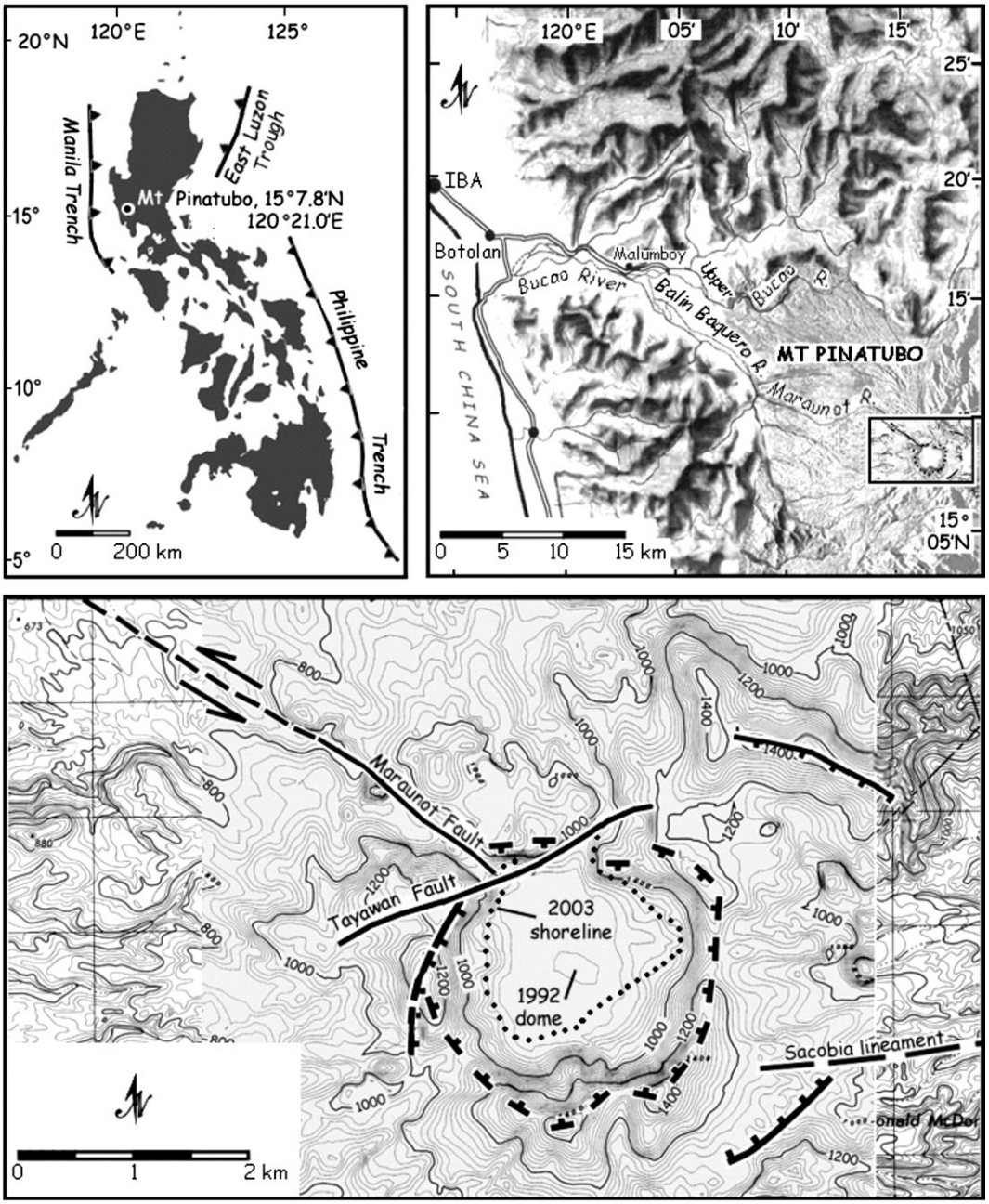


Fig. 5. Map of Pinatubo volcano showing the present (inner hatched curve) and ancient caldera (outer hatched curve) rims and major structural features of the volcano. The Maraunot Fault intersects the northwest rim of the present caldera lake (From Lagmay et al., 2007).

deposits have been found around this cone, indicating that no lateral collapse has occurred in the history of the volcano. The Kizimen case study demonstrates that: i) basement faults can propagate through an entire volcanic edifice, and hence basement-generated tectonic stresses do affect volcanoes; ii) active faulting, even when associated with strong earthquakes such as in the Kizimen area, is not sufficient to trigger lateral collapse, unless a large enough magma intrusion is produced within the volcano (Tibaldi et al., 2006). This will be further documented in the section devoted to analogue modelling.

### 2.5. Pinatubo (Philippines)

Pinatubo is an active volcano located in the Philippines arc, Luzon island. The basement is affected by a series of faults with a dominant NW–SE strike. The younger fault movements, Quaternary in age, are left-lateral strike–slip and localized along the Philippines fault system (Aurelio, 2000; Pasquarè and Tibaldi, 2003). The Quaternary tectonic state of stress, coeval with the development of Pinatubo, has been characterized by horizontal $\sigma_1$ and $\sigma_3$, consistent with a transcurrent setting (Bautista et al., 1996). The 1991 Pinatubo eruption deposited 5–6 $km^3$ of debris and pyroclastic deposits (Wolfe and Hoblitt, 1996) on the volcano slopes, much of which has been remobilized into large lahars in the following rainy seasons. A vertical collapse of the eruption column, localized in part along pre-existing faults, occurred on the volcano summit and left a caldera 2.5 km in diameter that almost immediately began to accumulate a $1.6\times10^8$ $m^3$ lake (Lagmay et al., 2007 and references therein). In this section, we will describe the geomorphological and structural conditions that accompanied the discharge of water from this lake and the erosion processes which took place along the volcano flank.

By 2001, the water level inside the summit caldera had risen to the Maraunot Notch, the lowest, northwestern portion of the caldera rim. That year, a narrow artificial canal, dug into an old volcanic breccia underlying the outlet channel of the Maraunot Notch, failed to induce a deliberate lake breakout. In July 2002, heavy rains caused the water to overflow naturally at the Maraunot Notch. This discharge produced erosion of this part of the caldera rim deepening the notch by 23 m, and as a consequence releasing an estimated $6.5\times10^7$ $m^3$ of lake water. This water bulked up into lahars with a volume well in excess of $1.6\times10^8$ $m^3$ that were the largest lahars ever to be generated by Pinatubo since its eruption in 1991 (Lagmay et al., 2007).

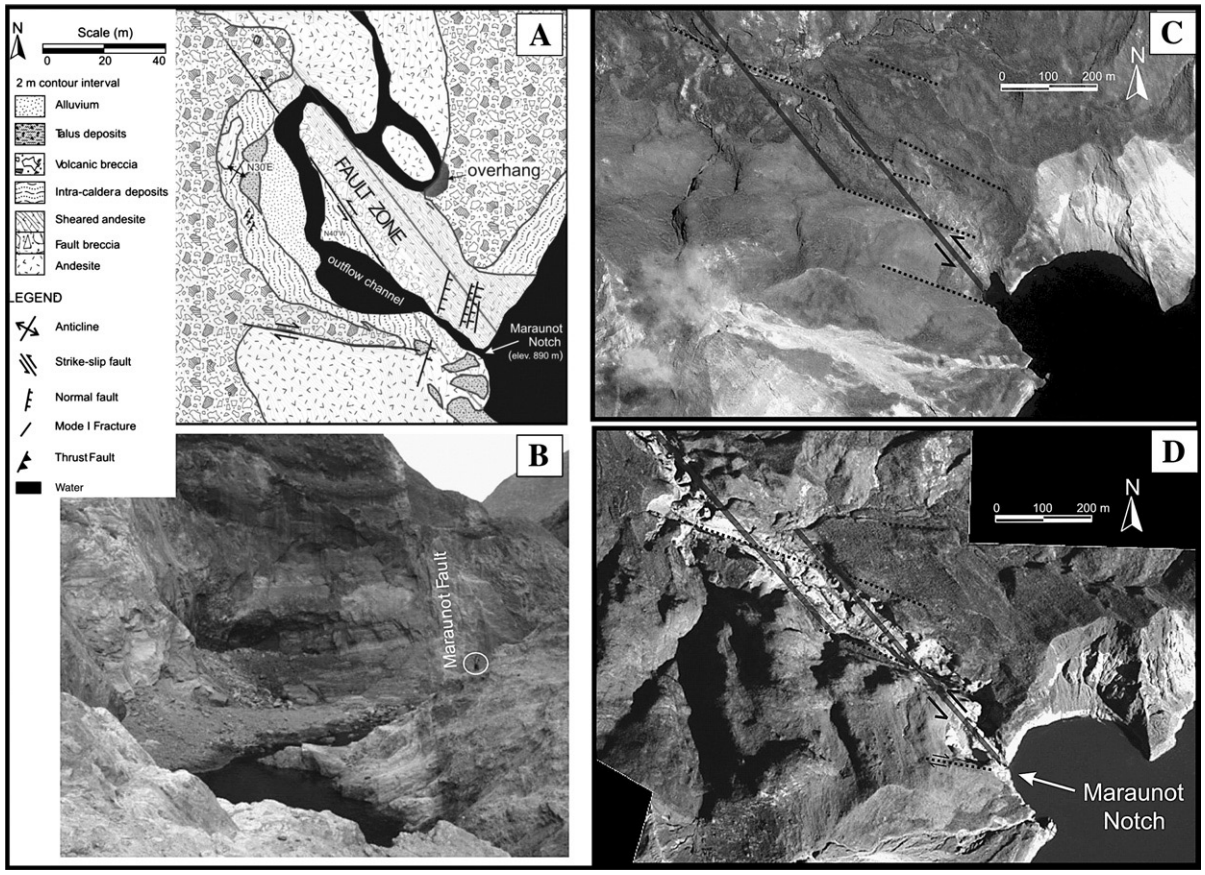


Fig. 6. A. Geologic map of the Maraunot Notch area, Pinatubo Volcano, Philippines. The Maraunot Fault zone strikes N40°W and is shown shaded over the contact between the lacustrine deposits and fault breccia. B. Northwestward view from within the Maraunot Notch of a major slip plane of the Maraunot Fault, which strikes N35°–40°W and dips steeply, separating the intra-caldera sedimentary deposits (left block) from the brecciated andesitic unit (right block). For scale, encircled is a man, 1.53 m tall, standing near the trace of the Maraunot fault at the centre-right portion of the image. C. Aerial views of the Maraunot Notch before the 2002 breaching event, the traces of the Riedel shears (dotted lines) of the Maraunot Fault (solid heavy lines) are evident in the Ikonos and aerial photos. D. The post-breach image shows scouring of the river channel, coincident with the trace of the Riedel shears in the pre-breach image (adopted from Lagmay et al., 2007).

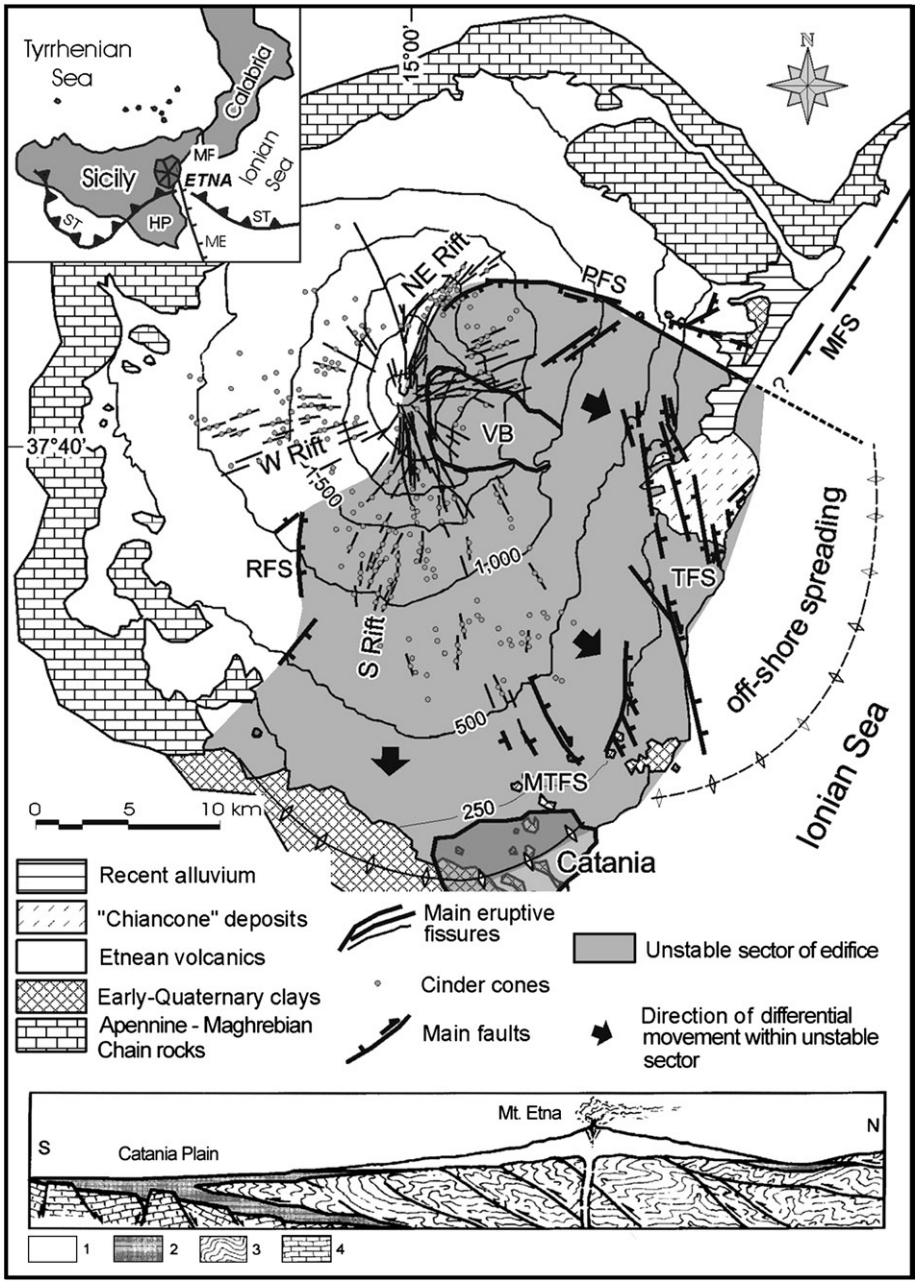


Fig. 7. Simplified geological map of Mt. Etna (Italy) showing the main structural features, including the three principal rift zones (NE, S and W) on the volcano and highlighting the unstable eastern and southern flanks. The southern and eastern fronts of the spreading are evident from deformation of sediments on the southern margin of Etna (Borgia et al., 1992, 2000a, b) and inferred from bathymetric data in the Ionian Sea (Borgia et al., 1992). RFS = Ragalna fault, MTFS = Mascalucia–Trecastagni fault system, PFS = Pernicana fault system, TFS = Timpe fault system, VB = Valle del Bove. Inset map: AI = Aeolian Islands, HP = Hyblean Plateau, ME = Malta Escarpment, MF = Messina fault system, ST = Sole thrust of the Appenine–Maghrebian Chain (rocks within the Chain are shown as Pre-Quaternary sedimentary rocks on the main map).

From a geological–structural perspective, the Maraunot Notch is controlled by the presence of the Maraunot Fault, an active, northwest-striking, left-lateral basement fault (Fig. 5). The fault's role in controlling erosion at the notch is manifested in several important physiographic features. The Maraunot Notch and the closest downstream channel into which lake water drains coincide with the site of a pre-1991 channel, carved because rocks were rendered less resistant to erosion by ancient tectonic movements along the Maraunot Fault. The breccia that was eroded away by the 2002 breakout is probably a landslide deposit that filled an ancestral Maraunot valley, also carved in rocks weakened by faulting. Thus, the Maraunot Notch is a relatively late physiographic expression that owes its existence to movements along the Maraunot Fault (Fig. 6A,B). Pre-breaching images of Pinatubo's northwest flank display lineaments that are "Riedel" shears of a major left-lateral fault (Fig. 6C). These lineaments helped to control the path taken by the water released during the breaching. After the deep scouring, the control of the Maraunot Fault on the morphology and structural character of the northwest flank was exposed even more clearly (Fig. 6D).

The volume of the lake remaining perched 1 km above sea level in the Pinatubo caldera is about $10^8$ $m^3$, and is thus regarded as a flash flood and lahar hazard. The control of the Maraunot Fault on the morphostructure of the notch still has major implications for such hazards. The notch and outlet channel owe their existence to weakness caused by past activity

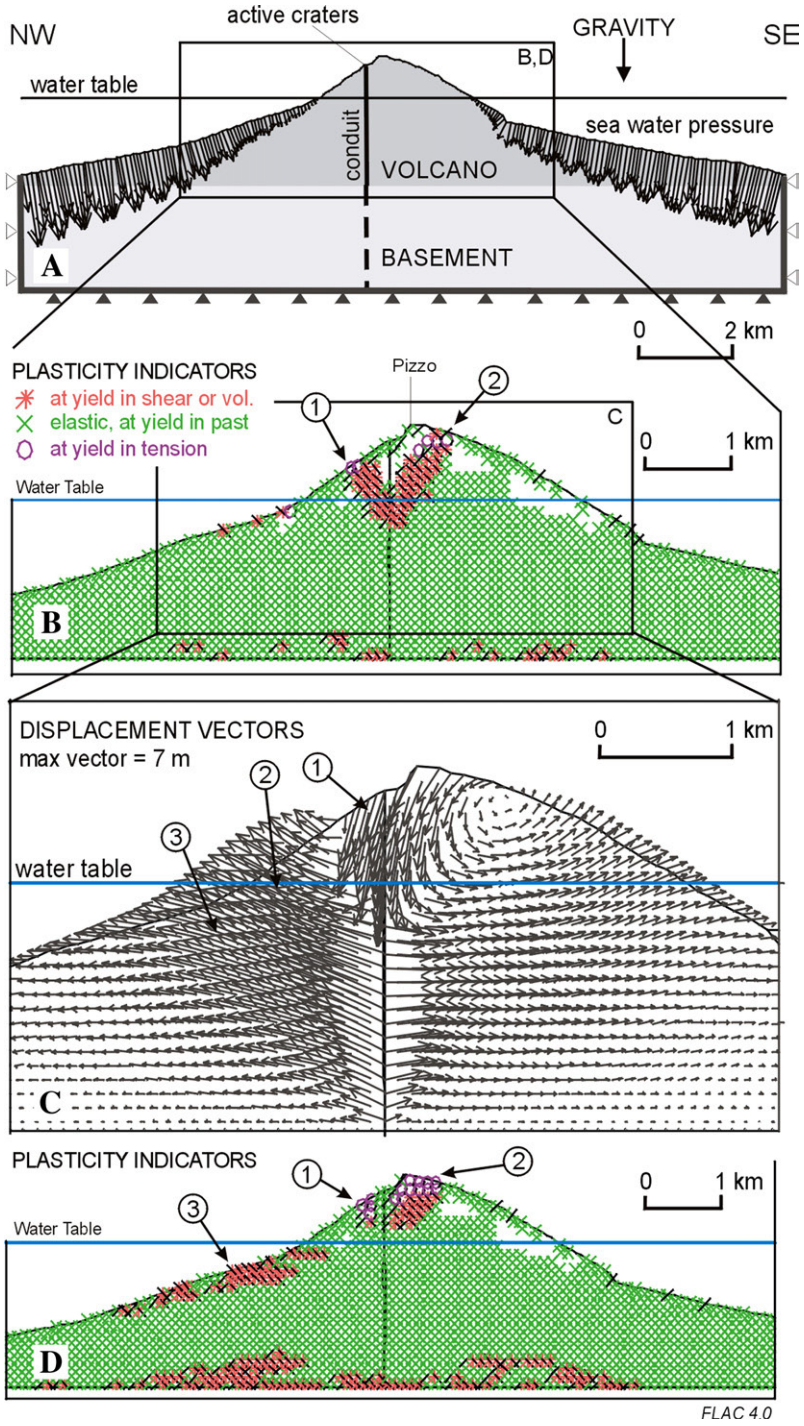


Fig. 8. A. Idealization of the system (substrate and volcanic edifice) for the key Stromboli site along a NW–SE cross-section, orthogonal to the main rift axis (cfr. Fig. 1). Material properties from Apuani et al. (2005a). Boundary conditions and applied external forces are represented. Dry conditions for the subaerial part of the volcano and a flat water table coincident with sea level were considered. The conduit trace is the bi-dimensional evidence of the NE-trending main rift zone, to which magma pressure is applied in terms of both magmastatic and overpressure components. B. Plasticity indicators developed as a consequence of the application of the magmastatic component along the feeding system. (1) and (2) indicate the areas at yield. C. Displacement vectors due to the application of the magmastatic component evidence: (1) vertical deformation above 500 m with the development of a summit active wedge with a vertical shear zone, (2) an outward horizontal deformation, and (3) a passive zone, indicating the possible emergence of a sliding surface at about −500 m. D. Plasticity indicators consequent on the additional application of an overpressure component along the feeding system. (1) The NW slope shows retrogressive development of plasticization in the upper part, and (2) the Pizzo area is subject to tension; (3) submarine shallow instabilities develop.

Table 1
Material properties used in the numerical model (from Corazzato, 2004 and Apuani et al., 2005b)

| DOMAIN | Constitutive model * | Cohesion c (Pa) | Friction angle $\phi$ (°) | Dilation angle (°) | Bulk volume $\gamma$ (kg/m$^3$) | Tensile strength (Pa) | Modulus of deformation $E_m$ (Pa) | Poisson's ratio $\nu$ | Bulk modulus $K$ (Pa) | Shear modulus $G$ (Pa) |
|---|---|---|---|---|---|---|---|---|---|---|
| Volcanic edifice | MC | 1.00E+06 | 35 | 0 | 1900 | 1.10E+04 | 2.00E+09 | 0.28 | 1.51E+09 | 7.81E+08 |
| Basement | E | – | – | – | 3000 | – | 6.00E+11 | 0.30 | 5.00E+11 | 2.31E+11 |

* E=elastic; MC=Mohr–Coulomb equivalents from Hoek–Brown.

along the fault. The plane of the Maraunot Fault, like those of other strike–slip faults, is steeply dipping. Governed by that tectonic fabric and accompanying structural weakness, the slopes of the outlet channel are steep and, along with many subvertical fractures, extend far above the channel floor, where lateral scour by stream flow is also a concern. This situation enhances the likelihood of channel-blocking landslides, lake rises, and breakouts.

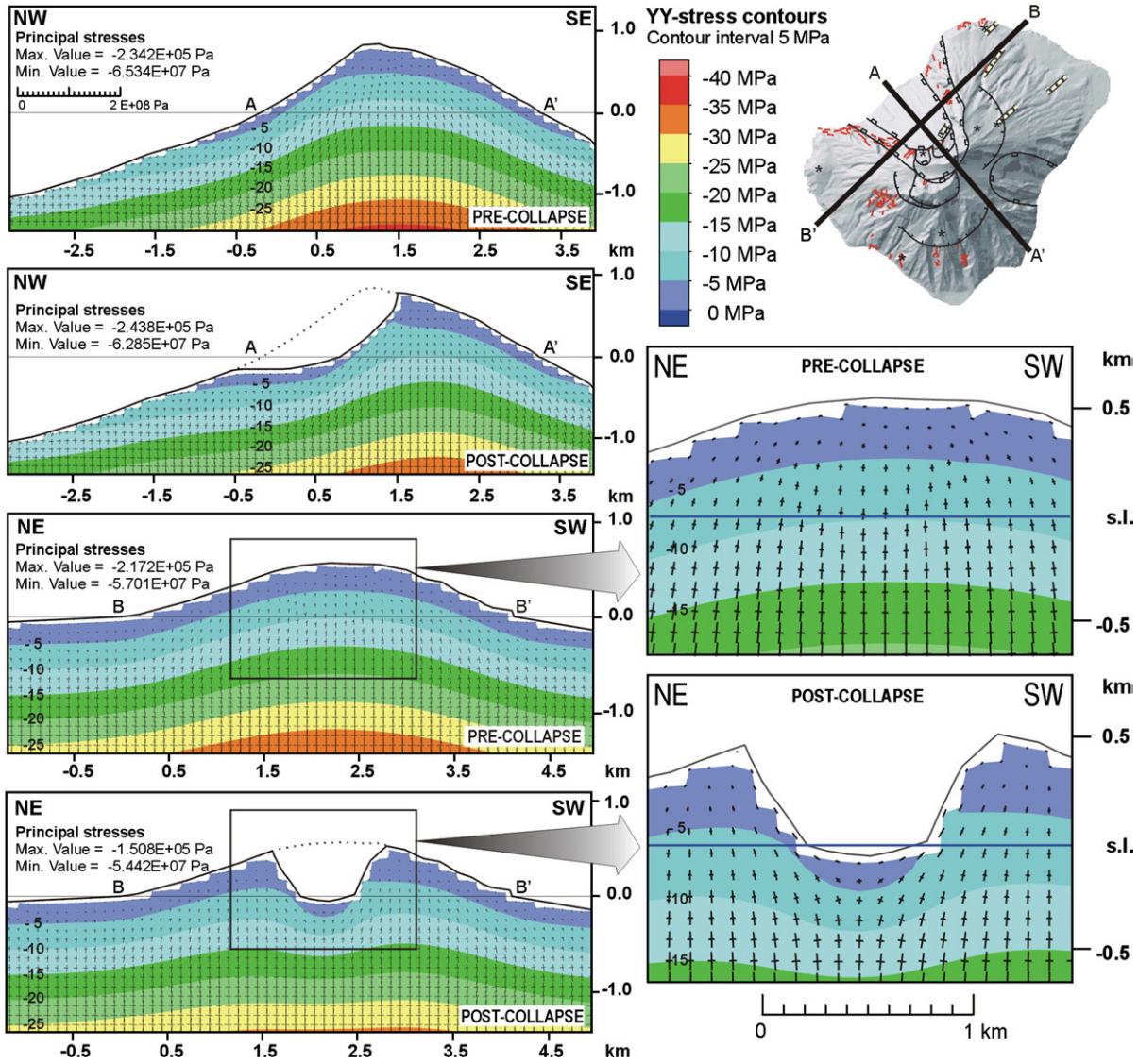


Fig. 9. Results of finite difference numerical modeling for the key Stromboli site, focusing on the reorganization in the stress distribution within the edifice after a lateral collapse, e.g. that of the Fossetta edifice (cfr. Fig. 2). On the left, NW–SE and NE–SW cross-sections, respectively parallel and orthogonal to the collapse scar, are presented (location in the upper right inset). For each of these, pre- and post-collapse stress configuration has been computed, in terms of both vertical stress contours and principal stress tensors (negative values indicate compression). A strong reorganization in the stress distribution occurs, both in terms of magnitude and orientation. A closer view (lower right) particularly demonstrates the marked reorientation of the stress tensors close to the collapse scarps, with the minimum compressive stress normal to the collapse surface. This local configuration favours the intrusion of dykes parallel to the collapse scarps and dipping at high angles towards the depression, and is consistent with field evidence.

### 2.6. Mt. Etna (Italy)

Mt. Etna is situated above the African–European plate boundary on the eastern margin of the Sicilian continental crust, a tectonic setting that imparts both structurally and lithologically complex discontinuities to the edifice substrate (Fig. 7). The volcano, Europe's largest (rising to about 3350 a.s.l.) and one of the most active, has arisen rapidly from a succession of overlapping central vents and associated flank eruptions in approximately the last 200 ka (Romano, 1982; Calvari et al., 1994; Coltelli et al., 1994; Corsaro et al., 2002; Branca et al., 2004). According to Lanzafame et al. (1997a), Barberi et al. (2000) and Patanè and Privitera (2001) the stress and strain field at Mt. Etna are homogeneous in the western sector at depths greater than 10 km; in particular, the main compressive stress and strain axes are almost horizontal and trending about N–S. The complexity of Etna's tectonic setting is enhanced by the fact that this N–S compressive regime in the lower crust coexists with an about ESE–WNW extensional regime (Monaco et al., 2005). The northern and western parts of the volcano overlie and are buttressed against a pre-existing topography developed in metamorphic and sedimentary rocks within a southward-verging system of thrusted nappes, the Apennine–Maghrebian Chain, at the southern margin of the Eurasian plate. By contrast, the southern and eastern flanks of the edifice overlie marine early Quaternary plastic clays that accumulated in the foredeep created on the tectonically depressed northern margin of the northward-dipping downgoing African plate (Lentini, 1982; Fig. 7). Field relationships between the Apennine–Maghrebian Chain rocks and the early Quaternary sub-Etnean clays indicate that thrusting continued until at least mid-Pleistocene times (Lanzafame et al., 1997b). Active regional uplift is indicated by outcrops of the early Quaternary marine clays that occur up to several hundred metres above sea level on the volcano flanks, and by Holocene reefs that are being uplifted at a rate of about 2 mm/yr along the Etnean coast (Firth et al., 1996; Rust and Kershaw, 2000).

From a structural perspective, the volcanic edifice of Etna is characterised by the presence of the NE, N–S and W rift zones, located in the upper part of the volcano slopes. These rifts are characterised by a concentration of eruptive fissures, pyroclastic cones, and main fracture systems. The more recent dykes and historical fissure eruptions and fractures mostly occurred along an arcuate zone, in plan view, passing through the volcano summit and open eastwards. Along the eastern lower volcano flank, the Timpe and Messina fault systems are of regional importance.

Numerous studies have proposed large scale sliding of the eastern and southern flanks of the volcano (Borgia et al., 1992; Lo Giudice and Rasà 1992; Rust and Neri, 1996; Garduño et al., 1997; Groppelli and Tibaldi, 1999; Borgia et al., 2000a,b; Froger et al., 2001; Tibaldi and Groppelli, 2002; Acocella et al., 2003; Neri et al., 2004; Rust et al., 2005; Corazzato and Tibaldi, 2006). The emerging picture is that the geological background outlined above sets the scene for complex edifice instability phenomena that are essentially unrecognised elsewhere. Most notable is the long record of relatively slow and steady sliding, albeit with limited accelerations associated with magma pressure, particularly from flank eruptions (Acocella et al., 2003; Rust et al., 2005). Movement on the northern boundary of the unstable mass, the Pernicana fault, averages up to about 2 cm/yr (Tibaldi and Groppelli, 2002), while the south-western boundary, the Ragalna fault, averages about 25% of this slip rate (Neri et al., 2007). The variability in these rates reflects the inhomogeneous nature of the instability, which presents a nested pattern of movement in both map and cross section views, with a series of basal detachments extending to a depth of at least 5 km (Rust et al., 2005). The position and strike of the Ragalna fault suggest that it is controlled by the rheological contrast between the juxtaposed rocks of the Chain and the sub-Etnean clays (Borgia et al., 1992; Rust and Neri, 1996; Fig. 7).

Finally, the Valle del Bove is a very large amphitheatre on the eastern flank of the volcano. This feature is generally regarded as being produced by a series of landslides feeding into debris flows now preserved as the late-Pleistocene to Holocene Chiancone sequence exposed on the coast east of Etna (Calvari et al., 1998; Fig. 7). The Valle del Bove lies close to the junction between the Timpe and Messina fault systems. The extent of the downfaulting is suggested by the depth of the Chiancone fault-bounded basin; this has been estimated as reaching 600 m on the basis of gravity surveys (Rollin, 1996).

## 3. Numerical modelling

In recent years, numerical modelling has been applied to volcano slope stability analyses, although this approach is still less common than in non-volcanic environments. Depending on the purpose, numerical modelling by finite difference codes (Kelfoun, 1999; Hurlimann, 1999; Hurlimann et al., 2000b; Apuani et al., 2005b), by distinct element codes (Zimbelman et al., 2003) or by finite element codes (Sousa and Voight, 1995; Russo et al., 1996; Hurlimann, 1999) have been applied. These analyses were often coupled with limit equilibrium methods (Voight et al., 1983; Iverson, 1995; Elsworth and Voight, 1996; Voight and Elsworth, 1997; Elsworth and Day, 1999; Voight, 2000; Hurlimann et al., 2000a,b; Donnadieu et al., 2001; Okubo, 2004; Apuani et al., 2005b).

In this paper, numerical modelling has been applied to enhance the understanding of general processes demonstrated by field data. Stromboli is investigated here, with the following goals. (1) Evaluate the control of substrate tectonics on the strain field and instability by modelling the role of magma pressure acting along a dyke swarm (whose surface expression is the rift zone) consistent with the NW–SE tectonic direction of extension. The geometry of this process guides the preferential magma intrusion path and formation of rift-zones, as well as controlling flank deformation and large-scale instability. (2) Investigate and quantify the changes in the stress field within the volcanic edifice once a lateral collapse has occurred, including the implications for new magma intrusion paths. A finite difference code (FLAC 4.0, Itasca) was used in our analysis. Physical and mechanical rock mass properties, including Mohr–Coulomb equivalent parameters (cohesion and friction angle) and rock mass elastic parameters, were based on in-situ and

laboratory tests summarized in Apuani et al. (2005a,b). We also refer to these authors for the modelling procedures.

The model and the outcomes concerning goal (1) of this study are presented in Fig. 8. The Stromboli system was represented with a finite difference grid (Fig. 8A) encompassing two main lithotechnical domains (substrate and volcanic edifice). The analysis is carried out along a NW–SE cross section passing through the Sciara del Fuoco depression and the volcano summit, orthogonal to the main rift axis (Fig. 1). Material properties have been used as reported in Table 1,

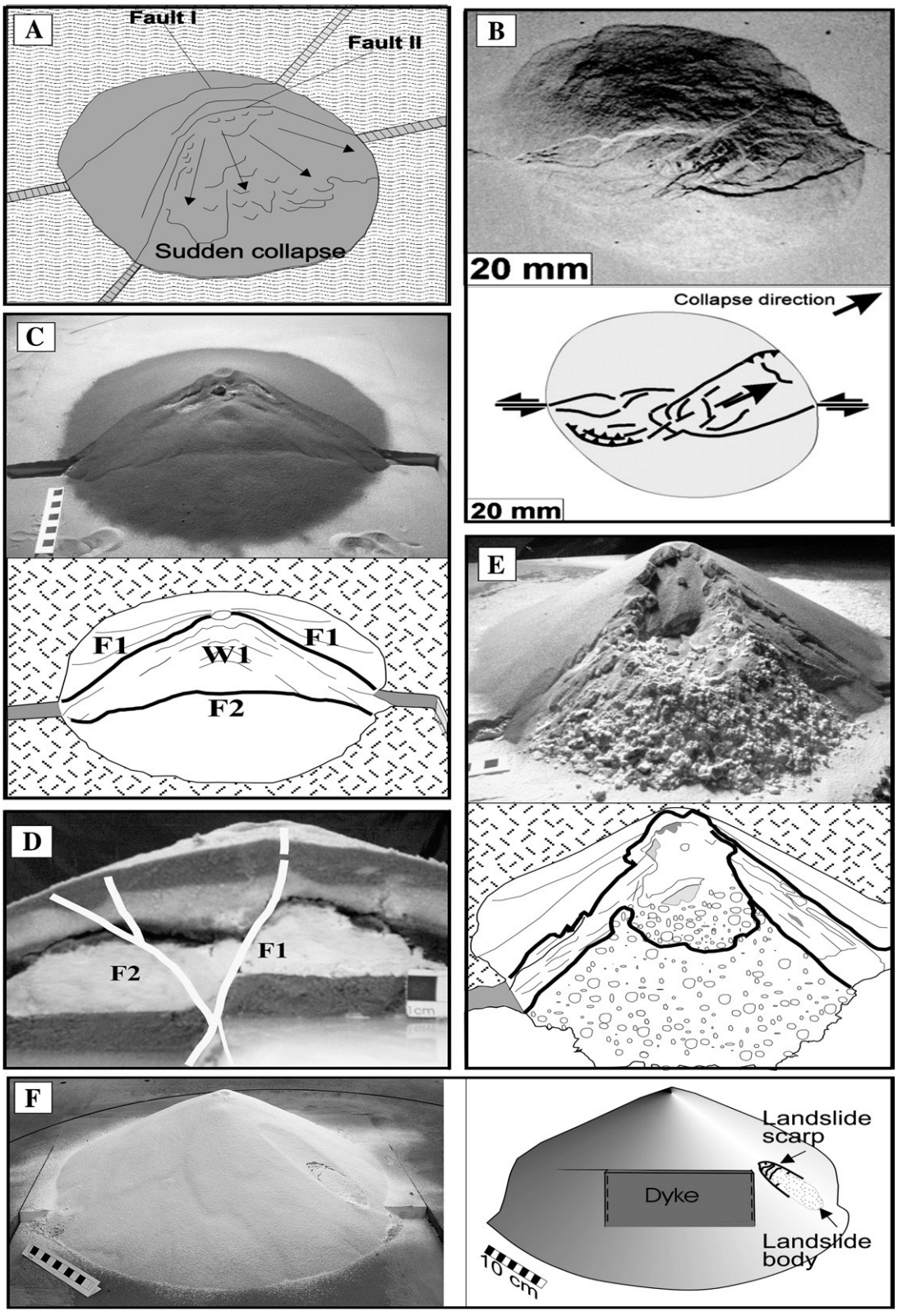

choosing the intermediate "Lava-Breccia lithotechnical unit" (Apuani et al., 2005a,b) to characterize the entire "volcanic edifice", with a Mohr–Coulomb constitutive model, while the substrate was assumed to be a rigid body for which an elastic constitutive model was chosen. Boundary conditions have been introduced, fixing element freedom of movement equal to zero at the base and side boundaries (black and white triangles). The extent of the section was chosen so that boundary conditions do not compromise the resulting stress–strain field in the area of interest (box). External forces on the submerged slope of the volcano, such as gravity and sea water load, have been applied. Dry conditions for the subaerial part of the volcano, and a flat water table coincident with sea level, were also modelled.

The trace of the conduit within the edifice, with a length of 2470 m, is the two-dimensional expression of the NE-trending main rift zone. Magma pressure was applied in terms of both magmastatic and overpressure components. The magmastatic component, defined as the static component due to the mean magma unit weight and the height of the dyke (Iverson, 1995), has a triangular distribution. A maximum value of 3.15E7 Pa was assumed for magmastatic pressure, based on considerations of both magma unit weight (Barberi et al., 1993), its variation and rock bridges (Corazzato, 2004). For the overpressure component, ranges suggested for the overpressure component by Rubin and Pollard (1987), Iverson (1995) and Delaney and Denlinger (1999) were used to select a value of 2.5E6 Pa.

Fig. 8B presents plasticity indicators developed as a consequence of the application of the magmastatic component along the feeding system, with the development of areas at yield stress. The displacement vectors (Fig. 8C) evidence: (1) vertical deformation above 500 m with the development of an active summit wedge with a vertical shear zone, (2) outward horizontal deformation, and (3) a passive zone, indicating the possible emergence of a sliding surface at approximately 500 m. Fig. 8D shows the plasticity indicators resulting from the additional application of an overpressure component along the feeding system. The NW slope shows retrogressive development of plasticization in the upper part (1), and the Pizzo area is subject to tension (2). Shallow submarine instabilities also develop (3).

The results concerning the second goal of numerical simulations are summarized in Fig. 9. NW–SE and NE–SW cross-sections were analyzed, respectively parallel and orthogonal to the collapse scar. For each section, the pre- and post-collapse stress configuration has been computed, in terms of both vertical stress contours and principal stress tensors (negative values indicate compression). It is evident that after lateral collapse, a strong reorganization in the stress distribution occurs within the edifice, both in terms of magnitude and orientation, on the order of several hundred metres from the collapse zone. In fact, an inflection in the contour lines (and thus a decrease in vertical stress) is observed below the collapse zone after the collapse event, following the debuttressing due to the removal of large rock masses. A closer view (to the right in Fig. 9) particularly illustrates the marked reorientation of the stress tensors close to the collapse depression, with $\sigma_3$ assuming a position perpendicular to the collapse escarpments. This local configuration favours the intrusion of dykes parallel to the collapse depression and dipping at high angles towards it. This result is consistent with field evidence, including those along the NE-rift of Stromboli controlled by substrate structures.

## 4. Analogue modelling

Analogue modelling has long been used to reproduce geological processes in the laboratory. We focus here on experiments conducted by several authors to model volcano instability caused by basement substrate heritage. Several model results have been selected, and these may be grouped in three categories: (1) examples of fault propagation from the basement into the volcanic edifice, (2) examples of the role played by the substrate in inducing volcano spreading and (3), examples of the mutual relationship between dyke propagation and volcano instability. Any experiment recreating natural volcanic systems must be carried out with appropriately scaled models (Hubbert, 1937; Ramberg, 1981), and a well-developed scaling methodology for dimensional analysis and materials has been established for experiments demonstrating volcano deformation (e.g. Tibaldi, 1995; Merle and Borgia, 1996; Vidal and Merle, 2000; Lagmay et al., 2000; Acocella, 2005). We refer to these papers for detailed explanations of the scaling procedure, methods and materials.

Several authors have used analogue modeling to investigate volcano instability due to basement faulting (Tibaldi, 1995; van Wyk de Vries and Merle, 1998; Lagmay et al., 2000; Vidal and Merle, 2000; Merle et al., 2001; Wooller et al., 2003, 2004). We hereby provide examples of fault propagation from the substrate to the volcanic edifice (category 1) that are derived from the work by Vidal and Merle (2000), Norini and Lagmay (2005) and Tibaldi et al., 2006. In the experiment shown in Fig. 10A, vertical faults offset the basement and a layered cone is used to simulate the presence of different rock types. The simultaneous reactivation of the two vertical faults in the basement (Vidal and Merle, 2000) generated two opposing faults at the model surface (Fault I and II in Fig. 10A) and a reverse fault whose presence was revealed by the tilting of layers within the model cone. Fault II and the reverse fault proved to be essential in destabilizing the cone flank, whereas Fault I played a minor role.

Fig. 10. Analogue modelling: A. Development of two opposing faults and sudden collapse of a heterogeneous model cone due to the simultaneous reactivation of two faults in the volcano's basement (modified after Vidal and Merle, 2000). B. Photograph (upper frame) showing development of superficial structures after 20 mm basal displacement. Sketch (lower frame) of surface features developed after 20 mm displacement (modified after Norini and Lagmay, 2005). C. Experimental results obtained after a 2-cm displacement; map view (modified after Tibaldi et al., 2006). D. Cross-section of the analogue cone showing the development of faults F1 and F2 with converging dip (modified after Tibaldi et al., 2006). E. Experiment using field parameters plus inflation with an inflatable bladder mimicking emplacement of the intermediate to acidic magmas of Ollagüe. The appearance of the cone after lateral collapse and debris avalanche development can be observed. Collapse in the actual edifice itself followed destabilization of the cone flank and further magma inflation in the cone (modified after Tibaldi et al., 2006). F. Dyke intrusion in a cone; note deformation on the flank along strike from the upwelling dyke (modified after Tibaldi et al., 2006).

Another instance, that of basement transcurrent faulting cutting across a modelled volcano (Fig. 10B), can yield well-developed fractures in the cone interior, although outwardly the edifice appears as a symmetrical cone, exhibiting concentric contours when viewed on a topographic map (Norini and Lagmay, 2005). Slight changes in the basal shape of the cone induced by strike–slip movements can be restored by the relatively faster resurfacing and reshaping processes from the deposition of younger eruptive products. This may be of key importance in terms of volcanic hazard assessment, since concealed deformation could induce instability in volcanoes and act as slip planes during lateral collapse events. Finally, lateral collapses can occur in a direction slightly oblique to the transcurrent fault strike.

When modelling (Tibaldi et al., 2006) deformation induced in a volcano by basement inclined normal faults, magma inflation and multiple flank deformation, experiments resulted in the development of a main fault (F1) cutting across the upper part of the cone below the summit crater and departing from the substrate fault with the same dip (Fig. 10C,D). A second curvilinear fault (F2) did develop from the substrate fault, but with opposite sense of dip. Significant deformation of the cone flank was recorded but no collapse occurred.

The effect of a shallow intrusion in the volcano's flank was then simulated by intruding the cone with an inflatable bladder. The case of no-previous structural destabilization, and the case of previous structural destabilization due to single substrate faulting, or repeated faulting alternating with cone growth, were both modelled. As shown in Fig. 10E, upon initial inflation of the bladder, a bulge (criptodome) formed in the central portion of the flank. The response of the analogue cone to this intrusion was the development of a catastrophic lateral collapse with a debris avalanche. Lateral collapse of the model cone occurred only when a shallow magmatic intrusion within the volcano was introduced. Fig. 10F shows a dyke intrusion across a volcano with consequent deformation along the fault strike, where the fissure eruption should occur at the stage of interception of the dyke with the topographic surface. A further outcome of these analogue experiments is that volcano flank deformation is enhanced if a previous flank destabilization occurred, interspersed with new cone growth.

Examples of the role played by the substrate structure in inducing volcano spreading (category 2), are taken from the works of Wooller et al. (2004) and Walter et al. (2006). The analogue basement, made of both ductile and brittle layers (Fig. 11A) was raised on one edge to introduce a substrate dip, above which the model cone was built. The resulting deformation and spreading were then analyzed as dips were increased. Another key role in triggering failure in downslope spreading volcanoes is played by basal thrusting, produced where a lateral constraint on ductile layers occurs (Fig. 11A). Walter et al. (2006) investigated the deformation of large volcanic edifices built by the coalescence of adjacent cones, by reproducing the spreading of an edifice composed of overlapping volcanoes. The results illustrate the following two main relationships between the spreading of overlapping volcanoes and the geometry (Fig. 11B) of new rift zones: (a) Spreading edifices of similar age that partially overlap tend to develop a rift zone approximately perpendicular to the boundary of both volcanoes, and this causes the two edifices to grow together and develop an elongated topographic ridge. (b) Partially overlapping volcanoes of different ages that spread at different rates form a rift zone that is parallel to their boundary, causing the two edifices to structurally separate from each other.

Examples of mutual relationships between dyke propagation and volcano instability (category 3), are taken from the works of Acocella and Tibaldi (2005) and Walter and Troll (2003). Acocella and Tibaldi (2005) used analogue experiments to investigate how dykes propagate across a volcano with a lateral collapse depression. The injections formed dykes that, away from the collapse depression, became radial (Fig. 11C). However, the dykes propagating near the collapse focused towards the collapse sides, becoming sub-parallel to them, indicating that the stress reorientation is due to unbuttressing. Only the dykes formed along the collapse axis (passing through the mid-line of the collapse in map view) were able to propagate radially within the collapse area.

Walter and Troll (2003) studied how a creeping volcanic flank may influence the evolution of rift zones. Their conclusion is that three main types of rift zone configuration may develop from an initially radial volcanic cone (Fig. 11D). Low eccentricity of the creeping sector (Fig. 11E) produces dyke intrusions along two curved axes tangential to the stable/unstable interface. In contrast, strong eccentricity of the creeping sector results in only one main tangential rift (Fig. 11F), while other rifts remain poorly developed or strike–slip faults develop. A diffuse dyke swarm is encouraged (Fig. 11G) in the sliding direction if edifice deformation is almost entirely by creep.

## 5. Discussion

Volcanologists have traditionally deciphered volcanic evolution by studying the physicochemical characteristics of the eruptive products, which are tightly linked with the physicochemical evolution of the magma feeding systems (e.g. Tanguy et al., 1997; Hobden et al., 2002). The volume of ascending magma, intruded/erupted ratio, explosive/effusive ratio, and lava rheology, are all parameters dependent on magma properties. More recently, it has been recognized that the geological, geomorphological and structural evolution of a volcano can also depend upon a series of feedback mechanisms occurring in the uppermost crust, i.e. in the volcano substrate or volcanic edifice (van Wyk de Vries and Borgia, 1996; Thouret, 1999; Borgia and van Wyk de Vries, 2003; Tibaldi et al., 2006). The following seeks to elucidate these feedback phenomena.

### *5.1. Substrate tectonics, rift zones and location of flank eruptions*

In extensional regimes, it is widely accepted that magma flow paths are linked to the regional tectonic stress field. This type of stress regime produces brittle discontinuities perpendicular to the least principal stress ($\sigma_3$) through which magma is transferred to the surface.

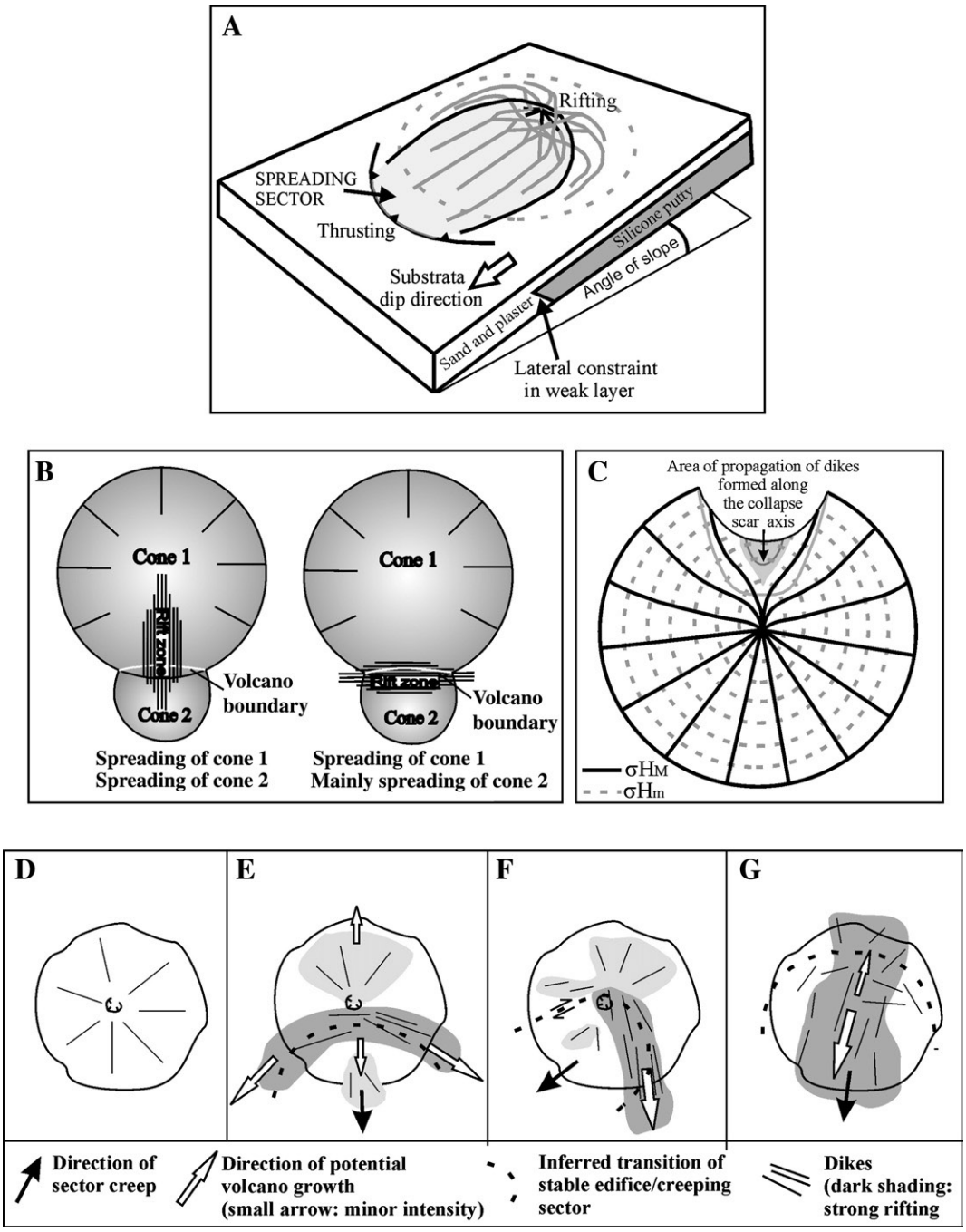


Fig. 11. A. Sketch of one of the possible slope-spreading processes, resulting from the introduction of a substrata slope to the analogue model. The downslope spreading of volcano and substrata is illustrated: Deformation occurs downslope until lateral discontinuity of weak substratum, where a thrust fault develops. Deformation and thrusting are confined to downslope sector (light shading), generating conditions for future lateral collapse (modified after Wooller et al., 2004). B. Sketch illustrating the two main trends of rift zones on overlapping volcanic edifices. Left: perpendicular to the boundary of both volcanoes. Right: parallel to the boundary of both volcanoes (Modified after Walter et al., 2006). C. Map view of an ideal cone with a collapse scar, showing the paths of dykes related to the distribution of stresses and the location of the collapse scar (modified after Acocella and Tibaldi, 2005). D–G. Main types of rift zone configurations that may develop from an initially radial volcanic cone. See text for details (modified from Walter and Troll, 2003).

Both Stromboli and Ollagüe volcanoes are characterized by a pre-lateral collapse stage during which a rectilinear volcanic rift zone crosscuts the cone. At Stromboli regional extension is NW–SE (Ferrari and Manetti, 1993; Tibaldi et al., 2003) and the rift zone trends NE–SW, whereas at Ollagüe regional extension is NE–SW (Feeley et al., 1993) and the rift trends NW–SE. In both cases, thus, the rift zone trends parallel to regional normal faults and perpendicular to the regional tectonic $\sigma_3$. These data suggest that the regional stress field can cause a preferred orientation in rift zones channelling magma up to the summit zone of the cone and feeder dyke swarms. In extensional regimes, the regional stress field can control the structure of the entire volcanic edifice. The analogue experiment with a dyke intruding into a volcano offset by a normal fault (Fig. 10F),

demonstrates that flank eruptions are expected at the intersection between the dyke and topography. Similar results were suggested on a theoretical basis from Nakamura et al. (1977), who showed that in many arc volcanoes island elongation and rifts are parallel with the trajectory of motion of the plate on which they are situated, suggesting that these rift zones are tectonically controlled. Detailed study of the Azores and Samoa also show the positions and orientations of rift zones to be mainly tectonic in origin (Walker, 1999); more examples of volcanic rift zones parallel to basement normal faults have been found in Cappadocia, Turkey (Toprak, 1988), in the central Mexican Volcanic Belt (Pasquarè et al., 1988) and in Iceland (Takada, 1994). Seamounts aligned with basement faults also imply some effect of tectonic features on eruption geometry (Batiza and Vanko, 1983; Fornari, 1987). Our data thus, integrated with these literature examples, suggest that in extensional tectonic settings, inception and geometry of volcanic rift zones might be mostly controlled by substrate regional tectonics.

In the other studied volcanoes located in transcurrent tectonic settings (Pinatubo) or compressional cordilleran settings (Planchon), rift zones have not been recognized before the lateral collapse occurrence. In these cases, the regional tectonic state of stress has been characterised by a horizontal greatest principal stress ($\sigma_1$). Similar situations are present, for example, also at the Reventador (Tibaldi, 2005a) and Cotopaxi (Tibaldi, 2005b) volcanoes in Ecuador, at Galeras Volcano in Colombia (Tibaldi and Romero-Leon, 2000) and at the Trohunco and the Los Cardos–Centinela volcanic complexes in Argentina (Folguera et al., 2006b; Miranda et al., 2006). These data suggest that the lack of a clear rift zone might be due to a regional tectonic $\sigma_1$ acting in the horizontal plane, inhibiting the formation of a volcanic rift. Hence, we believe that in transcurrent/compressional tectonic settings more studies are necessary in order to understand the controls on the location of flank eruptions.

Finally, in case of large volcanoes resting above a ductile substrate, such as Mt. Etna which grew above clay sediments, rift formation can be related to the build-up of a local extensional stress field within the volcano by its weight (Borgia et al., 1992). In fact, in the general case of a zone of weakness underlying a volcano, gravity sliding or volcanic spreading have been proposed to control volcanic rifting and structural evolution (e.g. Borgia et al., 2000a,b); Fiske and Jackson (1972) suggested that rift zones in volcanoes such as the Hawaiian Islands do not generally coincide with basement structures; in the latter case, volcano loading and related stress distribution govern shallow rift formation.

### 5.2. Lateral collapses

The destructive power of volcanic lateral collapses was dramatically demonstrated by the 1980 lateral collapse of Mount St. Helens, in which 2.8 km$^3$ of debris travelling at a speed of 35 m/s (was spread over an area of 60 km$^2$ (Voight et al., 1981). Although collapse of volcanic cones is most commonly associated with composite volcanoes (Ui, 1983), catastrophic slope failure is not limited to steep-sided volcanoes (Siebert, 1996). Massive slumps and debris avalanches are now widely recognised on gently-inclined subaerial and submarine volcano slopes in many basaltic volcanic islands. Examples include the Hawaiian, Reunion, Tristan de Cunha, Canary, Marquesas, and Galapagos islands (Lenat et al., 1989; Chadwick et al., 1991; Holcomb and Searle, 1991; Moore et al., 1994). Debris avalanches entering the sea can generate destructive tsunamis, which cause most of the fatalities associated with volcanic lateral collapse (Siebert, 1996). These hazards emphasize the importance of understanding the parameters governing the geometry and triggering of lateral collapses, as discussed in this section.

#### 5.2.1. The role of the volcanic substrate

Data from Mt. Etna illustrate the importance of the inherited recent and currently active tectonic structures and substrate geology in guiding collapse geometry. The generally southeastwards sliding direction and the steady-state sliding character of the movement appear to be determined by a combination of: 1) the lithologic boundary between the flysch sequence belonging to the Apennine–Maghrebian Chain and the Quaternary marine clay deposits, and the resulting rheological contrast, being orientated approximately normal to the sliding direction, and 2) the unbuttressing of the eastern flank of the volcano, where the Sicilian continental crust is truncated by the Malta Escarpment and related structures. In outcrop the sub-Etnean clays are pervasively affected by a network of apparently conjugate fractures whose surfaces exhibit slickensiding. Whether this is related to the sliding, or to late thrusting of the Apennine–Maghrebian Chain rocks, or a combination of both, is difficult to determine. However, these small-scale structures do indicate that deformation in the clays tends to be distributed, rather than localized along discreet structures, a characteristic that can be expected to apply to a greater extent in the subsurface where confining pressures and water content promote distributed plastic deformation This interpretation suggests that the distinctive stable sliding of Etna arises from cohesion and frictional drag in the clays underlying the unstable sector. By contrast, all the other cases studied in this paper suggest that instability occurring entirely within the volcanic edifice is likely to produce sudden and potentially catastrophic movement as the elastic limit of the rocks is exceeded, particularly since these relatively competent volcanic lithologies are unlikely to exert a sliding effect on the moving mass in the same way as the Etnean clays. If this analysis is correct, it suggests that Etna may not be prone to the hazards of deep-seated lateral collapse, although shallower failures within the volcanics remain a threat.

At Stromboli and Ollagüe, the collapse direction is perpendicular to the trend of dykes and of regional structures. In fact, lateral collapses developed perpendicularly to the rift zones, towards the NW and SE at Stromboli and towards the SW at Ollagüe. The development of major lateral collapses in these directions at Stromboli and Ollagüe can be interpreted as due to the effect of dip of the substrate in those directions. Also, at Mt. Etna, the Valle del Bove depression, as well as the sliding

direction of the whole eastern flank, developed eastwards, perpendicular to the main N–S orientation of the summit rift zone. This is consistent with the results of previous studies regarding extensional settings, where flank instability occurs on the hanging wall after propagation of basement normal faults across the cone, as here demonstrated by analogue modelling and field data at Ollagüe. Along these extensional structures, intrusive sheets can propagate exerting a lateral push on the volcano flank. This magma push has been widely accepted to destabilize the volcano flank (Siebert et al., 1987; Tibaldi, 1996, 2001; Voight and Elsworth, 1997; Voight, 2000; Donnadieu et al., 2001). In the case of transcurrent basement tectonics, analogue modelling also indicates that collapse direction is mainly controlled by the orientation of the fault, being slightly oblique to the fault strike (Fig. 8B). With a compressional cordilleran setting (Planchon), the lateral collapse direction is perpendicular to the dominant N–S structural grain of the basement.

All these data suggest that in volcanoes where gravitational spreading is absent, collapse geometry is controlled by basement topography (i.e. the dip of the basement) and tectonics, both directly in the case of normal or transcurrent faulting, or indirectly through the formation of a tectonically-controlled rift zone. As a consequence, active basement faulting can be used to predict the volcano flanks prone to lateral instability, and the direction of possible failure. In the case of spreading volcanoes, analogue modelling suggests that rift zone formation and instability leading to lateral collapse are primarily controlled by the distribution of the weak substrate and the topographic gradient (Walter and Troll, 2003). Consequently, the location and orientation of potential lateral collapse can also be assessed for these volcanic edifices.

#### 5.2.2. The role of climate

Lateral collapses at extinct volcanoes are believed to be triggered by seismic shaking and/or heavy rains with consequent increase of water pore pressure (Tibaldi et al., 1995; McGuire, 1996; Voight and Elsworth, 1997; Kerle et al., 2003). Since most volcanic regions are located in humid environments (e.g. Central America, Northern Andes, Alaska–Aleutian–Kamchatka–Kurile belt, Indonesia, Philippines, New Zealand, and most oceanic island volcanoes), the combination of rain and seismic events can create the conditions for widespread landsliding, as was observed during the 1987 $M_s$ 6.1–6.9 earthquakes in Ecuador, when more than 2000 landslides were triggered in the Reventador volcanic area (Tibaldi et al., 1995). Therefore, the combination of endogenous and exogenous processes can produce very hazardous conditions.

The sensitivity of landslide formation to water content and ground saturation suggests that climate change is also likely to affect the stability of volcanic environments in the future. It is likely that those areas where climate change scenarios predict more intense rainfall will be subject to a greater incidence of volcanic landsliding. The sensitivity of more temperate volcanic regions (e.g. Mediterranean area, Japan) to this factor also suggests a potential climate-induced increase in landslide hazard in these areas. Capra (2006) notes that during the last 30,000 years, major lateral collapses have occurred during periods of rapid deglaciation. Volcanoes with existing summit glaciers may also be subject to a greater incidence of landsliding and lahars as a result of global warming. Melting of a stabilizing glacial cover increases the water pressure in the summit deposits, and destabilizes oversteepened slopes.

#### 5.2.3. The role of magma pathways

Magma pressure strongly contributes to triggering lateral collapse in active volcanic areas (e.g. Apuani et al., 2005b). Several large lateral collapses have been triggered by magma inflation in the cone (Elsworth and Voight, 1995; Iverson, 1995; Elsworth and Voight, 1996; McGuire, 1996). Since magma inflation occurs along dyke swarms (whose surface expression are the rift zones) that can be geometrically guided by regional tectonic fractures and/or stress fields, it follows that regional tectonics might also control collapse triggering. At Planchon, the development of a shallow magma chamber preceded the lateral collapse, although it cannot be shown that the two were causally linked.

Pathways of magma flow to the surface can change after a lateral collapse. All the field examples considered here, as well as analogue and numerical modelling, indicate that a migration of dykes and eruptive centres can occur after lateral collapse. At both Stromboli and Ollagüe, a rectilinear zone of magma upwelling developed before the lateral collapse. Subsequently, at Stromboli, dykes became re-orientated to align with the Sciara del Fuoco collapse depression. The location of post-collapse volcanic activity also concentrated along and within the collapse depression at Ollagüe and Planchon. This phenomenon was first described by Tibaldi (1996) as a general process, whereas re-orientation of single intrusions was also noticed at Mt. Etna by McGuire et al. (1990). Analogue modelling experiments (Acocella and Tibaldi, 2005) suggest that, if the intrusion starts within the depression, dyking will propagate throughout it. On the other hand, if dyking starts close to the depression but outside it, dyking will propagate along the collapse scarps. Numerical modelling presented here explains this pattern as both a rotation and a magnitude change of stress tensors after a lateral collapse. Vertical stresses decrease and rotate, with $\sigma_3$ assuming a position perpendicular to the collapse escarpments. This reorganization can therefore be ascribed to unbuttressing of the collapse zone following removal of the large mass of rock. Unbuttressing resulting from the collapse depression itself can also affect the stress distribution, and thus magma paths, on the order of a few hundred metres from the active centre. Other authors demonstrate that rift zones in volcanoes re-align following lateral collapses and gravitational spreading (Tibaldi, 2001; Walter and Troll, 2003; Tibaldi, 2004; Acocella and Tibaldi, 2005; Walter et al., 2006; Münn et al., 2006). Since rift zones are structural features where dykes preferentially intrude and eruptions take place, it follows that lateral collapses and the location of eruption centres are intimately linked.

If, instead of being distributed along a dyke swarm, magma upwelling concentrates in one main conduit, a new cone can grow within the collapse depression. This possibility is

confirmed at Stromboli and Planchon, where the main central crater zone migrated a few hundred metres after the lateral collapse developed.

#### 5.2.4. The role of volcano height

Finally, among the factors determining the likelihood of a lateral collapse, we must also consider volcano height. At Stromboli, each main collapse occurred when the cone reached a similar altitude, on the order of 800–1100 m a.s.l. (3300–3600 above the sea floor). Ollagüe collapsed when it reached about 2000 m in height above the substrate, and Planchon when at least 1600 m above the substrate. St. Augustine volcano, in Alaska, collapsed laterally several times as it reached about the same altitude (Beget and Kienle, 1992). If a critical height is not reached, then only rare conditions, such as very large magma intrusions, can induce collapse. This height control may explain why Kizimen has not yet collapsed, since it has only very recently reached an altitude of 1500 m. Kizimen does have a substrate with a strong gravity gradient, due to offset along the graben faults, but this has apparently not yet been sufficient to induce lateral collapse. Notably, this is despite a series of large-magnitude earthquakes following major faulting in the area (Kozhurin et al., 2006). Kizimen does not show evidence of dyking, since there are no flank eruptive centres or eruptive fractures; suggesting that magma upwelling probably occurred along a stable central conduit. Moreover, the mass of the volcano itself has not been enough to impede vertical magma upwelling, i.e. horizontal migration or internal segregation of magma has not been favoured up to now. The role of substrate tectonics in this situation could be important in triggering eruptions, given the likely correlation between duration of volcanic cycles and return period of fault movements.

### 5.3. Landslides and erosion

Volcanic regions are prone not only to hazards derived from catastrophic lateral collapse events, but also to smaller landslides, volcanic mudflows (lahars), and debris flows. Considering the timescales of these phenomena, lateral collapses can occur with a frequency on the order of 30 to a few hundred years in a volcanic group with a high magma production rate (Tibaldi et al., 2005), whereas landslides, lahars, and debris flows have a much higher frequency. Except for pyroclastic flows, lahars are the most devastating volcanic processes on active volcanoes (Thouret, 1999).

Scott et al. (2001) note that, in general, catastrophic volcanic debris flow avalanches and landslides are fundamentally related to the presence of large volumes of structurally weak and potentially water-saturated material underlying steep slopes at high altitudes in tectonically active zones. All the volcanoes described here are deeply dissected, even though they are all young and active. Erosion processes at Stromboli, which is only 100 ka old, have exhumed the inner magma feeding system and deeply dissected the flanks of the cone which have not been affected by lateral collapses. The role of substrate tectonics in this case could be important in triggering eruptions along Stromboli's southern flank, where most rock mass removal has occurred through surface landsliding and slow erosion. It is noteworthy that these processes occur along the older NE–SW-trending rift zone on Stromboli. At Ollagüe, deep, wide canyons have been excavated by slow erosion processes along the northwestern and southeastern cone flanks, that is, along the old NW–SE-trending rift zone. At Planchon, lateral collapse and landslides have exposed the inner core of the volcanic system while, at Pinatubo, erosion as a result of water escape from the summit caldera lake was guided through the Maraunot Notch, that is, along a first order fault crossing the volcano. At Mt. Etna, large-scale deformation at the lower eastern flank is linked with movements produced along the rift zone. The formation of the Valle del Bove, through a series of landslides and debris flows (Calvari et al., 1998) could have been triggered by tectonic movements along the Timpe and Messina fault systems. Relative downfaulting by some 600 m on the easternmost flank of the volcano, taking place on these structures, increases the potential for gravity-driven collapses; as does periodic inflation and oversteepening on the summit slopes of the volcano. Consequently, the denudation processes that took place at Mt. Etna appear to be characterised as a series of rapid debris flows concentrated in a relatively short time span. In contrast, present erosion in the Valle del Bove occurs at a very slow rate.

Finally, hydrothermal alteration of volcanoes can play a fundamental role in guiding exogenous erosion processes; such is the case for example at Ollagüe and Planchon. However, hydrothermal activity is also controlled by the structures along which fluids propagate. These structures can be tectonic in origin, and thus linked to the substrate tectonic heritage, or they can derive from the structural reorganization of a volcano following a lateral collapse; events that are themselves typically guided by substrate tectonics and/or subsurface rheology.

All the studied examples indicate that volcanic–tectonic features such as rift zones, and tectonic structures such as faults, directly control the extent, location and geometry of the zones prone to landslides and slower erosion processes. Knowledge of a volcano's structural history and that of its substrate allows prediction of the locus of specific erosion processes.

## 6. Conclusions

The field examples given in this paper show that in composite volcanoes not subject to gravity spreading, substrate tectonic structures control pre-lateral collapse magma pathways, large lateral collapses, smaller landslide events, and preferential erosion. The tectonic crustal stress state or the presence of substrate fractures can determine the geometry of volcanic rift zones, which in turn guide the direction of large lateral collapse. In zones of active extension, tectonically-controlled rift zones preferentially develop, as shown in the case of Stromboli and Ollagüe. Also in a compressional cordilleran setting like at Planchon volcano, the orientation of lateral collapse can be controlled by the dominant substrate faults. In all these cases, the orientation of the collapse is normal to fault strike, and in turn depends on the general dip of the substrate. Analogue and numerical modelling confirm these data and interpretations.

The field data presented here also show that erosion and surface landslides can follow the strike of faults affecting volcanic edifices or rift zones, giving rise to preferential zones of degradation on the cone flanks and summit. In the case of summit crater lakes, tectonics can guide the erosional breaching of the crater rim with consequent production of lahars, as seen at Pinatubo.

Once a lateral collapse occurs, the related debuttressing produces a reorganization of the rift zone to produce a horseshoe-shaped arrangement in plan view. This theory is confirmed by analogue and numerical modelling, and by the field data at Stromboli, Ollagüe and Mt. Etna. Migration of the main magma conduit towards the collapse depression can occur after a lateral collapse, as demonstrated at Stromboli, Ollagüe and Planchon.

When a weak substrate is present under a volcano, as at Mt. Etna, long-lasting, deeply-rooted creeping phenomena can occur, deforming a large sector of the cone. This deformation, in turn, can induce more surficial landslides that propagate along the destabilized flank axis.

In the absence of a rift zone, as seen in the Pinatubo area affected by transcurrent faults, the propagation of the fault from the substrate across a volcano can induce flank destabilization oblique to fault strike. This destabilization likely evolves into lateral collapse if other mechanisms are involved, such as strong seismic motion or shallow magmatic intrusion.

The data presented here demonstrate clear relationships between substrate tectonics and flank eruption, lateral collapse, and erosion. Accordingly, detailed analysis of substrate and edifice structure provides a fundamental component of volcanic hazard assessment.

## Acknowledgments

This study was performed in the framework of the ILP project "New tectonic causes of volcano failure and possible premonitory signals". This work benefits of grants by the Istituto Nazionale di Geofisica e Vulcanologia–Gruppo Nazionale per la Vulcanologia; Italian Ministry of Instruction, University and Research; Philippine Council for Advanced Science and Technology Research; National Geographic Society (USA); Russian Foundation for Basic Research. Exchange visits of Italian and Russian scientists promoting cooperative research were funded by NATO—Russia Collaborative Linkage grant JSTC.RCLG.978989.

## References

Acocella, V., 2005. Modes of sector collapse of volcanic cones: insights from analogue experiments. J. Geophys. Res. 110, B02205. doi:10.1029/2004JB003166.

Acocella, V., Tibaldi, A., 2005. Dyke propagation driven by volcano collapse: a general model tested at Stromboli, Italy. Geophys. Res. Lett. 32, L08308. doi:10.1029/2004GL022248.

Acocella, V., Behncke, B., Neri, M., D'Amico, S., 2003. Link between major flank slip and eruptions at Mt. Etna (Italy). J. Geophys. Res. 30, 2286. doi:10.1029/2003GL018642.

Acocella, V., Vezzoli, L., Omarini, R., Matteini, M., Mazzuoli, M., 2007. Kinematic variations across Eastern Cordillera at 24°S (Central Andes): tectonic and magmatic implications. Tectonophysics 434, 81–92.

Apuani, T., Corazzato, C., Cancelli, A., Tibaldi, A., 2005a. Physical and mechanical properties of rock masses at Stromboli: a dataset for flank instability evaluation. Bull. Eng. Geol. Environ. 64, 419–431. doi:10.1007/s10064-005-0007-0.

Apuani, T., Corazzato, C., Cancelli, A., Tibaldi, A., 2005b. Stability of a collapsing volcano (Stromboli–Italy): limit equilibrium analysis and numerical modelling. In: Gudmundsson, A., Acocella, V. (Eds.), The Tectonics and Physics of Volcanoes. J. Volcanol. Geotherm. Res., vol. 144, pp. 191–210. 1–4.

Aurelio, M.A., 2000. Shear partitioning in the Philippines: constraints from Philippine Fault and global positioning system data. The Island Arc 9 (4), 584–597.

Barberi, F., Rosi, M., Sodi, A., 1993. Volcanic hazard assessment at Stromboli based on review of historical data. Acta Vulcanol. 3, 173–187.

Barberi, G., Cocina, O., Neri, G., Privitera, E., Spampinato, S., 2000. Volcanological inferences from seismic-strain tensor computations at Mt. Etna Volcano, Sicily. Bull. Volcanol. 62, 318–330.

Batiza, R., Vanko, D., 1983. Volcanic development of small oceanic central volcanoes on the flanks of the East Pacific Rise inferred from narrow-beam echo-sounder surveys. Mar. Geol. 54, 53–90.

Bautista, B.C., Bautista, M., Stein, R., Barcelona, E., Punongbayan, R., Laguerta, E., Rassdas, A., Ambubuyog, G., Amin, E., 1996. Relationship of regional and local structures to Mount Pinatubo activity. In: Newhall, C.G., Punongbayan, R.S. (Eds.), Fire and Mud: Eruptions and Lahars of Mount Pinatubo, Philippines. PHIVOLCS, Quezon City. University of Washington Press, Seattle, WA, pp. 351–370.

Beget, J.E., Kienle, J., 1992. Cyclic formation of debris avalanches at mount St Augustine volcano. Nature 356, 701–704.

Bermúdez, A., Delpino, D., 1989. La Provincia Basáltica Andino Cuyana. Asociación Geológica Argentina, Revista 44, 35–55.

Billi, A., Barberi, G., Faccenna, C., Neri, G., Pepe, F., Sulli, A., 2006. Tectonics and seismicity of the Tindari Fault System, southern Italy: crustal deformations at the transition between ongoing contractional and extensional domains located above the edge of a subducting slab. Tectonics 25, TC2006. doi:10.1029/2004TC001763.

Borgia, A., van Wyk de Vries, B., 2003. The volcano-tectonic evolution of Concepciòn, Nicaragua. Bull. Volcanol. 65 (4), 248–266.

Borgia, A., Ferrari, L., Pasquarè, G., 1992. Importance of gravitational spreading in the tectonic and volcanic evolution of Mount Etna. Nature 357, 231–235.

Borgia, A., Delaney, P.T., Denlinger, R.P., 2000a. Spreading volcanoes. Ann. Rev. Earth Planet. Sci. 28, 539–570.

Borgia, A., Lanari, R., Sansosti, E., Tesauro, M., Berardino, P., Fornaro, G., Neri, M., Murray, J.B., 2000b. Actively growing anticlines beneath Catania from the distal motion of Mount Etna's decollment measured by SAR interferometry and GPS. Geophys. Res. Lett. 27, 3409–3412.

Braitseva, O.A., Melekestsev, I.V., Ponomareva, V.V., Sulerzhitsky, L.D., 1995. The ages of calderas, large explosive craters and active volcanoes in the Kuril–Kamchatka region, Russia. Bull. Volcanol. 57 (6), 383–402.

Branca, S., Coltelli, M., Groppelli, G., 2004. Geological Evolution of Etna Volcano. In: Bonaccorso, A., Calvari, S., Coltelli, M., Del Negro, C., Falsaperla, S. (Eds.), Etna Volcano Laboratory, AGU (Geophysical monograph series), pp. 49–63.

Capra, L., 2006. Abrupt climactic changes as triggering mechanisms of massive volcanic collapses. J. Volcanol. Geotherm. Res. 155, 329–333.

Calvari, S., Groppelli, G., Pasquarè, G., 1994. Preliminary geological data on the south-western walls of Valle del Bove, Mt. Etna (Sicily). Acta Vulcanol. 5, 15–30.

Calvari, S., Tanner, L.H., Groppelli, G., 1998. Debris–avalanche deposits of the Milo Lahar sequence and the opening of the Valle del Bove on Etna volcano (Italy). J. Volcanol. Geotherm. Res. 87 (1–4), 193–209.

Chadwick Jr., W.W., De Roy, T., Carrasco, A., 1991. The September 1988 intracaldera avalanche and eruption at Fernandina volcano, Galapagos Islands. Bull. Volcanol. 53, 276–286.

Clavero, J., Sparks, R.S.J., Aguilar, G., van Wyk de Vries, B., 2004. Substrata influence in the origin, transport and emplacement of Ollagüe debris avalanche, Central Andes of northern Chile. Acta Vulcanol. 16 (1–2), 59–76.

Coltelli, M., Garduño, V.H., Neri, M., Pasquarè, G., Pompilio, M., 1994. Geology of northern wall of Valle del Bove, Etna (Sicily). Acta Vulcanol. 5, 55–68.

Corazzato, C., 2004. A quantitative study of volcano lateral collapses: the example of Stromboli (Italy). PhD thesis, Università di Milano–Bicocca, Italy, 154 pp.

Corazzato, C., Tibaldi, A., 2006. Fracture control on type, morphology and distribution of parasitic volcanic cones: an example from Mt. Etna, Italy. J. Volcanol. Geotherm. Res. 158, 177–194.

Corsaro, R., Neri, M., Pompilio, M., 2002. Paleo-environmental and volcano-tectonic evolution of the south-eastern flank of Mt. Etna during the last 225 ka inferred from volcanic succession of the «Timpe», Acireale, Sicily. J. Volcanol. Geotherm. Res. 72, 1–19.

Davidson, J., 1974. A Quaternary volcanic mudflow (lahar) down the Claro and Teno valleys from Planchon Volcano. International Symposium on Volcanology, Santiago, Abstracts of papers, pp. 14–15.

Davidson, J., de Silva, S.L., 1992. Volcanic rocks from the Bolivian Altiplano: insights into crustal structure, contamination, and magma genesis in the central Andes. Geology 20, 1127–1130.

de Silva, S.L., 1989. Altiplano–Puna volcanic complex of the Central Andes. Geology 17, 1102–1106.

de Silva, S.L., Francis, P.W., 1991. Volcanoes of the Central Andes. Springer–Verlag, Berlin, p. 216.

de Silva, S.L., Self, S., Francis, P.W., Drake, R.E., Ramirez, R.C., 1994. Effusive silicic volcanism in the Central Andes the Chao dacite and other young lavas of the Altiplano–Puna Volcanic Complex. J. Geophys. Res. 99 (B9), 17805–17825.

Delaney, P.T., Denlinger, R.P., 1999. Stabilization of volcanic flanks by dyke intrusion: an example from Kilauea. Bull. Volcanol. 61, 356–362.

Donnadieu, F., Merle, O., Besson, J.-C., 2001. Volcanic edifice stability during cryptodome intrusion. Bull. Volcanol. 63, 61–72.

Elsworth, D., Day, S., 1999. Flank collapse triggered by intrusion: the Canarian and Cape Verde Archipelagoes J. Volcanol. Geotherm. Res. 94 (1–4), 323–340.

Elsworth, D., Voight, B., 1995. Dike intrusion as a trigger for large earthquakes and the failure of volcano flanks. J. Geophys. Res. 100, 6005–6024.

Elsworth, D., Voight, B., 1996. Evaluation of volcano flank instability triggered by dyke intrusion. In: McGuire, W.J., Jones, A.P., Neuberg, J. (Eds.), Volcano instability on the Earth and other planets. Geol. Soc. London Spec. Publ., vol. 110, pp. 45–53.

Feeley, T.C., Davidson, J.P., 1994. Petrology of calc-alkaline lavas at Volcan Ollagüe and the origin of compositional diversity of central Andean stratovolcanoes. J. Petrol. 35, 1295–1340.

Feeley, T.C., Davidson, J.P., Armendia, A., 1993. The volcanic and magmatic evolution of Volcan Ollagüe, a high-K, late Quaternary stratovolcano in the Andean Central Volcanic Zone. J Volcanol. Geotherm. Res. 54, 221–245.

Ferrari, L., Manetti, P., 1993. Geodynamic framework of the Tyrrhenian volcanism: a review. Acta Vulcanol. 3, 1–9.

Firth, C., Stewart, I., McGuire, W.M., Kershaw, S., Vita-Finzi, C., 1996. Coastal elevation changes in eastern Sicily: implications for volcano instability at Mount Etna. In: McGuire, W.M., Jones, A.P., Neuberg, J. (Eds.), Volcano Instability on the Earth and Other Planets. Geol. Soc. London Spec. Publ., vol. 110, pp. 153–167.

Fiske, R.F., Jackson, E.D., 1972. Orientation and growth of Hawaiian volcanic rifts: the effect of regional structure and gravitational stresses. Proc. R. Soc. London 329, 299–326.

Folguera, A., Zapata, T., Ramos, V., 2006a. Late Cenezoic extension and the evolution of the Neuquen Andes. In: Kay, S.M., Ramos, V.A. (Eds.), Evolution of an Andean margin: A tectonic and magmatic view from the Andes to the Neuquén Basin (35°–39°S lat). Geol. Soc. Am. Spec. Paper, vol. 407, pp. 267–285.

Folguera, A., Ramos, V.A., Gonzalez Diaz, E.F., Hermanns, R., 2006b. Miocene to Quaternary deformation of the Guanacos fold-and-thrust belt in the Neuquén Andes between 37°S and 37°30′S. In: Kay, S.M., Ramos, V.A. (Eds.), Evolution of an Andean margin: A tectonic and magmatic view from the Andes to the Neuquén Basin (35°–39°S lat). Geol. Soc. Am. Spec. Paper, vol. 407, pp. 247–266.

Fornari, D.J., 1987. The geomorphic and structural development of Hawaiian submarine rift zones. In: Decker, R.W., Wright, T.L., Stauffer, P.H. (Eds.), Volcanism in Hawai`i. U.S. Geol. Surv. Prof. Pap., vol. 1350, pp. 125–132.

Francis, P.W., Wells, G.L., 1988. Landsat Thematic Mapper observations of debris avalanche deposits in the Central Andes. Bull. Volcanol. 50, 258–278.

Froger, J., Merle, O., Briole, P., 2001. Active spreading and regional extension at Mount Etna imaged by SAR interferometry. Earth Planet. Sci. Lett. 187, 245–258.

Gabbianelli, G., Romagnoli, C., Rossi, P.L., Calanchi, N., 1993. Marine geology of the Panarea–Stromboli area (Aeolian Archipelago, southeastern Tyrrhenian Sea). Acta Vulcanol. 3, 11–20.

Garduño, V.H., Neri, M., Pasquarè, G., Borgia, A., Tibaldi, A., 1997. Geology of the NE-rift of Mount Etna (Sicily, Italy). Acta Vulcanol. 9 (1/2), 91–100.

Gillot, P.-Y., Keller, J., 1993. Radiochronological dating of Stromboli. Acta Vulcanol. 3, 69–77.

Groppelli, G., Tibaldi, A., 1999. Control of rock rheology on deformation style and slip-rate along the active Pernicana fault, Mt. Etna, Italy. Tectonophysics 305, 521–537.

Hildreth, W., Fierstein, J., Godoy, E., Drake, R., Singer, B., 1999. The Puelche volcanic field: Extensive Pleistocene rhyolite lava flows in the Andes of central Chile. Rev. Geol. de Chile 26, 275–309.

Hobden, B.J., Houghton, B.F., Nairn, I.A., 2002. Growth of a young, frequently active composite cone: Ngauruhoe volcano, New Zealand. Bull. Volcanol. 64 (6), 392–409.

Holcomb, R.T., Searle, R.C., 1991. Large landslides from oceanic volcanoes. Mar. Geotech. 10, 19–32.

Hornig-Kjarsgaard, I., Keller, J., Koberski, U., Stadlbauer, E., Francalanci, L., Lenhart, R., 1993. Geology, stratigraphy, and volcanological evolution of the island of Stromboli, Aeolian Arc, Italy. Acta Vulcanol. 3, 21–68.

Hubbert, M.K., 1937. Theory of scale models as applied to the study of geologic structures. Geol. Soc. Am. Bull. 48, 1459–1519.

Hurlimann, M., 1999. Geotechnical analysis of large volcanic landslides: the La Orotava events on Tenerife, Canary Islands. PhD thesis, Technical University of Catalonia, 217 pp.

Hurlimann, M., Garcia-Piera, J.O., Ledesma, A., 2000a. Causes and mobility of large volcanic landslides: application to Tenerife, Canary Islands. J. Volcanol. Geotherm. Res. 103 (1–4), 121–134.

Hurlimann, M., Martì, J., Ledesma, A., 2000b. Mechanical relationship between catastrophic volcanic landslides and caldera collapse. Geophys. Res. Lett. 27, 2393–2396.

ITASCA, 2000. FLAC (Fast Lagrangian Analysis of Continua). User's guide. ITASCA Consulting Group, Minneapolis, MN.

Iverson, R.M., 1995. Can magma injection and groundwater forces cause massive landslides on Hawaiian volcanoes? J. Volcanol Geotherm. Res. 66 (1–4), 295–308.

Kay, S., Coira, B., Viramonte, J., 1994. Young mafic back arc volcanic rocks as indicators of continental lithospheric delamination beneath the Argentina Puna Plateau, Central Andes. J. Geophys. Res. 99 (B12), 24323–24339.

Kay, S., Godoy, E., Kurtz, A., 2005. Episodic arc migration, crustal thickening, subduction erosion, and magmatism in the south-central Andes. Geol. Soc. Amer. Bull. 117, 67–88.

Kelfoun, K., 1999. Lava dome growth and destabilization processes of Merapi volcano (Central Java, Indonesia). Numerical modelling of the domes, dynamics of associated pyroclastic flows and photogrammetric monitoring (In French). Ph.D Thesis, Univ. Clermond-Ferrand, 270 pp.

Kerle, N., van Wyk de Vries, B., Oppenheimer, C., 2003. New insight into the factors leading to the 1998 flank collapse and lahar disaster at Casita volcano, Nicaragua. Bull. Volcanol. 65 (5), 331–345.

Kozhurin, A.I., 2004. Active faulting at the Eurasian, North American and Pacific plates junction. Tectonophysics 380, 273–285.

Kozhurin, A., Acocella, V., Kyle, P.R., Lagmay, F.M., Melekestsev, I.V., Ponomareva, V., Rust, D., Tibaldi, A., Tunesi, A., Corazzato, C., Rovida, A., Sakharov, A., Tengonciang, A., Uy, H., 2006. Trenching studies of active faults in Kamchatka, eastern Russia: palaeoseismic, tectonic and hazard implications. Tectonophysics 417, 285–304.

Lagmay, A.M.F., van Wyk de Vries, B., Kerle, N., Pyle, D.M., 2000. Volcano instability induced by strike–slip faulting. Bull. Volcanol. 62, 331–346.

Lagmay, A.M.F., Rodolfo, K.S., Siringan, F.P., Uy, H., Remotigue, C., Zamora, P., Lapus, M., Rodolfo, R., Ong, J., 2007. Geology and hazard implications of the Maraunot Notch in the Pinatubo caldera, Philippines. Bull. Volcanol. 69 (7), 797–810.

Lanzafame, G., Neri, M., Coltelli, M., Lodato, L., Rust, D., 1997a. North–South compression in the Mt. Etna region (Sicily): spatial and temporal distribution. Acta Vulcanol. 9, 121–133.

Lanzafame, G., Leonardi, A., Neri, M., Rust, D., 1997b. Late overthrust of the Appenine–Maghrebian Chain at the NE periphery of Mt. Etna, Italy. C.R. Acad. Sc. Paris 324 (IIa), 325–332.

Lenat, J.F., Vincent, P., Bachelery, P., 1989. The offshore continuation of an active basaltic volcano: Piton de la Fournaise (Reunion Islands Indian Ocean). J. Volcanol. Geotherm. Res. 36, 1–36.

Lentini, F., 1982. The geology of the Mt. Etna basement. Mem. Soc. Geol. It. 23, 7–25.

Lipman, P.W., Moore, J.G., Swanson, D.A., 1981. Bulging of the north flank before the May 18 eruption — geodetic data. In: Lipman, P.W., Mullineaux, D.R. (Eds.), The 1980 eruptions of Mount St. Helens, Washington. U.S. Geol. Surv. Prof. Pap., vol. 1250, pp. 143–155.

Lo Giudice, E., Rasà, A., 1992. Very shallow earthquakes and brittle deformation in active volcanic areas: the Etnean region as an example. Tectonophysics 202, 257–268.

MacPhail, D., 1973. The geomorphology of the Rio Teno Lahar, Central Chile. Geographical Review 63, 517–532.

Mattioli, M., Renzulli, A., Menna, M., Holm, P.M., 2006. Rapid ascent and contamination of magmas through the thick crust of the CVZ (Andes, Ollagüe Region): evidence from a nearly aphyric high-K andesite with skeletal olivines. In: Tibaldi, A., Lagmay, A.F.M. (Eds.), Interaction between Volcanoes and their Basement. J. Volcanol. Geotherm. Res., pp. 87–105.

McGuire, W.J., 1996. Volcano instability: a review of contemporary themes. In: McGuire, W.J., Jones, A.P., Neuberg, J. (Eds.), Volcano instability on the Earth and other Planets. Geol. Soc. London Spec. Publ., vol. 110, pp. 1–23.

McGuire, W.J., Pullen, A.D., Saunders, S.J., 1990. Recent dyke-induced large-scale block movement at Mt. Etna and potential slope failure. Nature 343, 357–359.

Merle, O., Borgia, A., 1996. Scaled experiments of volcanic spreading. J. Geophys. Res. 101, 13805–13817.

Merle, O., Vidal, N., van Wyk de Vries, B., 2001. Experiments on vertical basement fault reactivation below volcanoes. J. Geophys. Res. 106, 2153–2162.

Miranda, F., Folguera, A., Leal, P.L., Naranjo, J.A., Pesce, A., 2006. Upper Pliocene to Lower Pleistocene volcanic complexes and Upper Neogene deformation in the south-central Andes (36° 30′–38°S). In: Kay, S.M., Ramos, V.A. (Eds.), Evolution of an Andean margin: A tectonic and magmatic view from the Andes to the Neuquén Basin (35°–39°S lat). Geol. Soc. Am. Spec. Paper, pp. 287–298.

Monaco, C., Catalano, S., Cocina, O., De Guidi, G., Ferlito, C., Gresta, S., Musumeci, C., Tortorici, L., 2005. Tectonic control on the eruptive dynamics at Mt. Etna volcano (eastern Sicily) during the 2001 and 2002–2003 eruptions. J. Volcanol. Geotherm. Res. 144, 221–233.

Moore, J.G., Albee, W.C., 1981. Topographic and structural changes, March–July 1980–Photogrammetric data. In: Lipman, P.W., Mullineaux, D.R. (Eds.), The 1980 eruptions of Mount St. Helens, Washington. U.S. Geol. Surv. Prof. Pap., vol. 1250, pp. 123–134.

Moore, J.G., Normark, W.R., Holcomb, R.T., 1994. Giant Hawaiian landslides. Annu. Rev. Earth Planet. Sci. 22, 119–144.

Münn, S., Walter, T.R., Klügel, A., 2006. Gravitational spreading controls rift zones and flank instability on El Hierro, Canary Islands. Geol. Mag. 143 (3), 257–268.

Nakamura, K., Jacob, K., Davies, J., 1977. Volcanoes as possible indicators of tectonic stress orientation – The Aleutians and Alaska. Pure Appl. Geophys. 115, 87–112.

Naranjo, J.A., Haller, M.J., 2002. Erupciones holocenas principalmente explosivas del Volcan Planchon, Andes del Sur (35 deg 15 min S). Rev. Geol. de Chile 29, 93–113.

Neri, M., Acocella, V., Behncke, B., 2004. The role of the Pernicana fault system in the spreading of Mt. Etna (Italy) during the 2002–2003 eruption. Bull. Volcanol. 66, 417–430.

Neri, M., Guglielmino, F., Rust, D., 2007. Flank instability on Mount Etna: radon, radar interferometry and geodetic data from the southern boundary of the unstable sector. J. Geophys. Res. 112, B04410. doi:10.1029/2006JB004756.

Norini, G., Lagmay, A.M.F., 2005. Deformed symmetrical volcanoes. Geology 33 (7), 605–608.

Okubo, C.H., 2004. Rock mass strength and slope stability of the Hilina slump, Kılauea volcano, Hawaii. J. Volcanol. Geotherm. Res. 138 (1–2), 43–76.

Pasquarè, G., Tibaldi, A., Attolini, C., Cecconi, G., 1988. Morphometry, spatial distribution and tectonic control of Quaternary volcanoes in northern Michoacan, Mexico. Rend. Soc. It. Min. Petr. 43 (4), 1215–1225.

Pasquarè, G., Francalanci, L., Garduno, V.H., Tibaldi, A., 1993. Structure and geological evolution of the Stromboli volcano, Aeolian islands, Italy. Acta Vulcanol. 3, 79–89.

Pasquarè, F., Tibaldi, A., 2003. Do transcurrent faults guide volcano growth? The case of NW Bicol Volcanic Arc, Luzon, Philippines. Terra Nova 15, 204–212.

Patanè, D., Privitera, E., 2001. Seismicity related to 1989 and 1991–93 Mt. Etna (Italy) eruptions: kinematic constraints by fault solution analysis. J. Volcanol. Geotherm. Res. 109, 77–98.

Ramberg, H., 1981. Gravity, Deformation and the Earth's Crust, 2nd ed. Academic Press, London.

Ramos, V., Cegarra, M., Cristallini, E., 1996. Cenozoic tectonics of the high Andes of west-central Argentina (30°–36.5°S). Tectonophysics 259, 185–200.

Riller, U., Petrinovic, I.A., Ramelow, J., Strecker, M.R., Oncken, O., 2001. Late cenozoic tectonism, collapse caldera and plateau formation in the Central Andes. Earth Planet. Sci. Lett. 188, 299–311.

Rollin, P., 1996. Geophysical models of Mount Etna, Sicily: its structural evolution and implications for slope stability. Unpubl. Doctoral dissertation, Open University. Author no. M7135588, BLDSC no. DXN11438.

Romano, R., 1982. Succession of the volcanic activity in the Etnean area. Mem. Soc. Geol. It. 23, 27–48.

Rubin, A.M., Pollard, D.D., 1987. Origin of blade-like dykes in volcanic rift zones. In: Decker, R.W., Wright, T.L., Stauffer, P.H. (Eds.), Volcanism in Hawaii. U.S. Geol. Surv. Prof. Pap., vol. 1350, pp. 1449–1470.

Russo, G., Giberti, G., Sartoris, G., 1996. The influence of regional stresses on the mechanical stability of volcanoes: Stromboli (Italy). In: McGuire, W., Jones, A.P., Neuberg, J. (Eds.), Volcano Instability on the Earth and Other Planets. Geol. Soc. London Spec. Publ., vol. 110, pp. 65–75.

Rust, D., Neri, M., 1996. The boundaries of large-scale collapse on the flanks of Mount Etna, Sicily. In: McGuire, W.C., Jones, A.P., Neuberg, J. (Eds.), Volcano Instability on the Earth and Other Planets. Geol. Soc. London Spec. Publ., vol. 110, pp. 193–208.

Rust, D., Kershaw, S., 2000. Holocene tectonic uplift patterns in northeastern Sicily: evidence from marine notches in coastal outcrops. Mar. Geol. 167, 105–126.

Rust, D., Behncke, B., Neri, M., Ciocanel, A., 2005. Nested zones of instability in the Mount Etna volcanic edifice, Sicily. J. Volcanol. Geotherm. Res. 155, 137–153.

Schmitz, M., Lessel, K., Giese, F., Wigger, F., Araneda, M., Bribach, J., Graeber, F., Grunewald, S., Haberland, C., Lüth, S., Röber, F., Ryberg, T., Schulze, A., 1999. The crustal structure beneath the Central Andean forearc and magmatic arc as derived from seismic studies — the PISCO 94 experiment in northern Chile (21°–23° S). J. South Am. Earth Sci. 12, 237–260.

Scott, K., Macias, J., Naranjo, J., Rodriguez, S., McGeehin, J., 2001. Catastrophic debris flows transformed from landslides in volcanic terrains: mobility, hazard assessment, and mitigation strategies. USGS Prof. Pap. 1630.

Shantser, A.E., Geptner, A.R., Egorova, I.A., Lupikina, E.G., Pevzner, M.A., Chelebaeva, L.I., 1969. Volcanologic strata of the Tumrok ridge, their paleomagnetic characteristics and age. Izv. AN SSSR. ser. geol. 9, 72–82 (in Russian).

Shantser, A.Ye., Kutyev, F.Sh., Petrov, V.S., Zubin, M.I., 1991. Kizimen volcano. Active volcanoes of Kamchatka, V.2. Nauka Publishers, Moscow, pp. 16–p.29.

Siebert, L., 1996. Hazards of large volcanic debris avalanches and associated eruptive phenomena. In: Scarpa, R., Tilling, R.I. (Eds.), Monitoring and Mitigation of Volcanic Hazards. Springer, New York, pp. 541–572.

Siebert, L., Glicken, H., Ui, T., 1987. Volcanic hazards from Bezymianny- and Banda-type eruptions. Bull. Volcanol. 49, 435–459.

Sousa, J., Voight, B., 1995. Multiple pulsed debris avalanche emplacement at Mount St. Helens in 1980: evidence from numerical continuum flow simulation. J. Volcanol. Geotherm. Res. 66, 227–250.

Takada, A., 1994. Development of a subvolcanic structure by the interaction of liquid-filled cracks. J. Volcanol. Geotherm. Res. 61, 207–224.
Tanguy, J.-C., Condomines, M., Kieffer, G., 1997. Evolution of the Mount Etna magma: constraints on the present feeding system and eruptive mechanisms. J. Volcanol. Geotherm. Res. 75 (3), 221–250.
Thouret, J.-C., 1999. Volcanic geomorphology—an overview. Earth-Sci. Rev. 47, 95–131.
Tibaldi, A., 1995. Morphology of pyroclastic cones and tectonics. J. Geophys. Res. 100 (24), 521–24,535.
Tibaldi, A., 1996. Mutual influence of diking and collapses at Stromboli volcano, Aeolian Arc, Italy. In: McGuire, W.C., Jones, A.P., Neuberg, J. (Eds.), Volcano Instability on the Earth and Other Planets. Geol. Soc. London Spec. Publ., pp. 55–63.
Tibaldi, A., 2001. Multiple sector collapses at Stromboli volcano, Italy: how they work. Bull. Volcanol. 63 (2/3), 112–125.
Tibaldi, A., 2004. Major changes in volcano behaviour after a sector collapse: insights from Stromboli, Italy. Terra Nova 16, 2–8.
Tibaldi, A., 2005a. Volcanism in compressional settings: is it possible? Geophys. Res. Lett. 32, L06309. doi:10.1029/2004GL021798.
Tibaldi, A., 2005b. Quaternary compressional deformation around the Cotopaxi Volcano, Ecuador. AGU Chapman conference on "The Effects of Basement, Structure, and Stratigraphic Heritages on Volcano Behaviour", 16–20 novembre 2005, Taal volcano, Tagaytay City, Philippines. abstract.
Tibaldi, A., Romero-Leon, J., 2000. Morphometry of Late Pleistocene-Holocene faulting in the southern Andes of Colombia and volcano-tectonic relationships. Tectonics 19 (2), 358–377.
Tibaldi, A., Groppelli, G., 2002. Volcano-tectonic activity along the structures of the unstable NE flank of Mt. Etna, Italy. J. Volcanol. Geotherm. Res. 115 (3–4), 277–302.
Tibaldi, A., Pasquaré, G., Francalanci, L., Garduño, V.H., 1994. Collapse type and recurrence at Stromboli volcano, associated volcanic activity, and sea level changes. Accademia dei Lincei, Atti dei Convegni Lincei, Roma 112, 143–151.
Tibaldi, A., Ferrari, L., Pasquarè, G., 1995. Landslide triggered by earthquakes and their relationships with faults and mountain slope geometry: an example from Ecuador. Geomorphology 11, 215–226.
Tibaldi, A., Corazzato, C., Apuani, T., Cancelli, A., 2003. Deformation at Stromboli volcano (Italy) revealed by rock mechanics and structural geology. Tectonophysics 361, 187–204.
Tibaldi, A., Lagmay, A.M.F., Ponomareva, V.V., 2005. Effects of basement structural and stratigraphic heritages on volcano behaviour and implications for human activities. Episodes 28 (3), 158–170.
Tibaldi, A., Bistacchi, A., Pasquarè, F., Vezzoli, L., 2006. Extensional tectonics and volcano lateral collapses: insights from Ollagüe volcano (Chile) and analogue modelling. TerraNova 18, 282–289.
Toprak, V., 1988. Neotectonic characteristics of the North Anatolian Fault Zone between Koyulhisar and Susehri (NE Turkey). METU J. Pure Appl. Sci. 21, 155–166.
Tormey, D., Frey, F., Lopez-Escobar, L., 1989. Geologic history of the active Azufre-Planchon-Peteroa volcanic center (35°15'S), with implications for the origin of compositional gaps. Revista de la asociacion Geologica Argentina XLIV, 420–430.
Tormey, D., Frey, F., Lopez-Escobar, L., 1995. Geochemistry of the active Azufre–Planchon–Peteroa volcanic complex, Chile (35°15'S): evidence for multiple sources and processes in a cordilleran arc magmatic system. J. Petrol. 36, 265–298.
Ui, T., 1983. Volcanic dry avalanche deposits—identification and comparison with non-volcanic stream deposits. J. Volc. Geoth. Res. 18, 135–150.
van Wyk de Vries, B., Borgia, A., 1996. The role of basement in volcano deformation. In: McGuire, W.C., Jones, A.P., Neuberg, J. (Eds.), Volcano instability on the earth and other planets. Geol. Soc. London Spec. Publ., pp. 95–110.
van Wyk de Vries, B., Merle, O., 1998. Extension induced by volcanic loading in regional strike–slip zones. Geology 26, 983–986.
Vidal, N., Merle, O., 2000. Reactivation of basement fault beneath volcanoes: a new model of flank collapse. J. Volcanol. Geotherm. Res. 99, 9–26.
Voight, B., 2000. Structural stability of andesite volcanoes and lava domes. Phil. Trans. R. Soc. Lond. 358, 1663–1703.
Voight, B., Elsworth, D., 1997. Failure of volcano slopes. Geotechnique 47 (1), 1–31.
Voight, B., Glicken, H., Janda, R.J., Douglass, P.M., 1981. Catastrophic rockslide avalanche of May 18. In: Lipman, P.W., Mullineaux, D.R. (Eds.), The 1980 eruptions of Mount St. Helens, Washington. U.S. Geol. Surv. Prof. Pap., vol. 1250, pp. 347–377.
Voight, B., Janda, R.J., Glicken, H., Douglass, P.M., 1983. Nature and mechanics of the Mount St Helens rockslide–avalanche of 18 may 1980. Geotéchnique 33, 243–273.
Walker, G.P.L., 1999. Volcanic rift zones and their intrusion swarms. J. Volcanol. Geotherm. Res. 94, 21–34.
Walter, T.R., Troll, V., 2003. Experiments on rift zone evolution in unstable volcanic edifices. J. Volcanol. Geotherm. Res. 127, 107–120.
Walter, T.R., Klügel, A., Münn, S., 2006. Gravitational spreading and formation of new rift zones on overlapping volcanoes. Terra Nova 18, 26–33.
Wolfe, E.W., Hoblitt, R.P., 1996. Overview of the eruptions. In: Newhall, C.G., Punongbayan, R.S. (Eds.), Fire and Mud: Eruptions and Lahars of Mount Pinatubo, Philippines. PHIVOLCS, Quezon City. University of Washington Press, Seattle, WA, pp. 3–20.
Wooller, L.K., Murray, J.B., Rymer, H., van Wyk de Vries, B., 2003. Volcano instability and collapse from basement faulting. *AGU–EUG–EGS*, Nice, France. Geophys. Res. Abstr. 5, 00304.
Wooller, L.K., van Wyk de Vries, B., Murray, J.B., Rymer, H., Meyer, S., 2004. Volcano spreading controlled by dipping substrata. Geology 32, 573–576.
Wörner, G., López Escobar, L., Moorbath, S., Horn, S., Entenmann, J., Harmon, R.S., Davidson, J.D., 1992. Variaciones geoquímicas, locales, yregionales, en el arco volcánico Andino del Norte de Chile (17°30'S–22°00'S). Rev. Geol. de Chile 19, 37–56.
Wörner, G., Hammerschmidt, K., Henjes-Kunst, F., Lezaun, J., Wilke, H., 2000. Geochronology (40Ar/39Ar, K-Ar and He-exposure ages) of cenozoic magmatic rocks from Northern Chile (18–22°S): implications for magmatism and tectonic evolution of the central Andes. Rev. Geol. de Chile 27, 205–240.
Zimbelman, D.R., Watters, R.J., Firth, I.R., Breit, G.N., Carrasco-Nuñez, G., 2003. Stratovolcano stability assessment methods and results from Citlaltépetl, Mexico. Bull. Volcanol. 66 (1), 66–79.